ADDIS ABABA UNIVERSITY

ADDIS ABABA INSTITUTEOF TECHNOLOGY

SCHOOL OF MECHANICAL AND INDUSTRIAL ENGINEERING

GRADUATE STUDIES

POST GRADUATE PROGRAM IN THERMAL ENGINEERING

Design, CFD Analysis, and Prototype Testing of Brim Diffuser Shrouded Horizontal Axis Wind Turbine

A thesis Submitted for the in partial fulfillment for the degree of masters of Science in Mechanical and Industrial Engineering (Thermal stream), in Addis Ababa University, Addis Ababa Institute of Technology (AAiT)

By:

Beshir Heyru Mohammed

Advisor:

Dr. Ing. Wondossen Bogale (Assistance Professor)

March 2020

Addis Ababa, Ethiopia

CERTIFICATION

I, the undersigned, certify that I read and hear by recommend for the acceptance by Addis Ababa University institute of Technology, Mechanical and Industrial Engineering (Thermal Engineering Stream) a thesis entitled "Design, CFD Analysis, and Prototype Testing of Brim Diffuser Shrouded Horizontal Axis Wind Turbine." This certificate used as a partial fulfillment of the requirement for the thermal engineering of Masters of Science in Mechanical Engineering.

Signature: ______________________

Date: _______________________

DECLARATION

I, Beshir Heyru, I declare that this thesis is the result of my own work and that all source or material used for this thesis have been duly acknowledged. This thesis is submitted in partial fulfillment of the requirement for Master's Degree in Thermal Engineering Stream at Addis Ababa University and to be made available at the university's Library under the role of the Library. I confidently declare that this thesis has not been submitted to any other institutions anywhere for the award of any academic degree, diploma, or certificate.

Signature: ________________________

Date: ________________________

Beshir Heyru

Addis Ababa University

Addis Ababa institute of Technology

School of Mechanical and Industrial Engineering Thermal Engineering Stream

Addis Ababa, Ethiopia

Design, CFD Analysis, and Prototype Testing of Brim Diffuser Shrouded Horizontal Axis Wind Turbine

By: Beshir Heyru

Approved by Board of Examiners:

Dr. Ing. Wondossen Bogale

(Advisor)	Signature	Date

Dr. Abdulkadir Aman

(Thermal Engineering Chair)	Signature	Date

Dr. Abdulkadir Aman

(External Examiner)	Signature	Date

Dr.Tilahun Nigussie

(Internal Examiner)	Signature	Date

Dr. Yilma Taddese

(Dean of School)	Signature	Date

Dr. Ermias Tesfaye

(Director of Post Graduate Program)	Signature	Date

ACKNOWLEDGMENT

First of all, I am thankful to my God, this research not possible without his blessing and helping. Then I would like to express my thankful to my advisor Dr. Ing. Wondossen Bogale for the continuous support of my master's study and research, for his motivation, passion, and sharing his knowledge and experience. His direction helped me in all the time of study and writing of this research. Besides my advisor, I would like to thank Mr. Natnaeil, for his help, understanding comments, and relevant questions.

Lastly, I would like to thank and appreciation for my friends for their peer review and guidance.

ABSTRACT

In lower wind speed regions, the generation of electrical power from conventional small-scale horizontal axis wind turbines is very difficult due to ineffective power extraction in lower wind speed. However, the introduction of a flanged diffuser that shrouds the wind turbine is used to increase and accelerate the wind speed that approach to wind turbine. This will permit extract efficient power at lower wind speed regions. This research addresses the design, optimization, model 3D Print or manufacturing, and experimental testing of a model diffuser augmented wind turbine.

2D CFD simulations were carried out to examine an optimum geometry of brim diffuser by utilizing different optimization techniques. All samples have the same dimensions in diffuser length, entrance area, exit area, and brim (or flange) length but they vary in sectional shape of diffuser and flange angles. Brim angles of these tested samples vary from -20^0 to 20^0 .The simulation shows that the curve sectional shape of a brimmed diffuser increases the velocity of the approaching wind speed by 7.06 % when compare to straight sectional shape. And also, from different flange angles for the curved sectional shape of brim diffuser, 10^0 flange angle improve the velocity augmentation by 4.07 % when compared to normal flange angel. Besides numerical result shows that the boundary layer flow separation points along inside of a diffuser greatly affect the acceleration of wind flow through a brimmed diffuser.

Subsequently, a MATLAB code is developed to optimize the blade twist angle and chord distributions. After this, the performance analysis of the optimized brim diffuser shrouded horizontal axis wind turbine is analyzed by using ANSYS- FLUENT. The CFD result shows that the optimized shrouded wind turbine increases the velocity and power augmentation by a factor of 1.58 and 3.78 respectively when compared to the performance of an unshrouded wind turbine with the same swept area and wind speed. Lastly, the prototype of shrouded turbine is manufactured and test its performance in the wind tunnel in the Addis Ababa Institute of Technology's laboratory. The experimental result is verified with numerical result with reasonable small deviation which will be suitable for the implementation of a shrouded turbine for lower wind speed regions for rural electrification.

Keywords: Augmentation; Brim diffuser; CFD; Optimized; Experimental testing; wind turbine.

List of Abbreviations, Symbols, and Nomenclature

C_p	Power coefficient
V_0	Downstream velocity
V_4	Free stream velocity
η_d	Diffuser efficacy
B	Number of blades
ε	Velocity ratio
γ	Diffuser speed up ratio
a	Axial induction factor
$a^{'}$	Agular induction factor
Ω	Rotational speed
λ	Tip speed ratio
ϕ	Relative wind angel
α	Angel of attack
U_{rel}	Relative wind velocity
C_l	Lift coefficient
C_d	Drag coefficient
β	Diffuser area ratio
C_t	Tangential force coefficient

C_n Normal force coefficient

L_t Total diffuser length

D_i Inlet diameter of diffuser

D_{throat} Throat diameter for diffuser

D_0 Outlet diameter for diffuser

D_{brim} Diameter of brim

h_{flange} Flange height

L_{shroud} Inlet shroud length

ABRIVATION

DAWT Diffuser Augmented Wind Turbine

CFD Computational Fluid Dynamics

SST Shear Stress Transport

AAiT Addis Ababa Institute of Technology

EBMT Extend Blade Element Momentum Theory

SSSBD Straight sectional shape of brim diffuser

CSSBD Curved sectional shape of brim diffuser

Table of Contents

List of Figures

List of Tables

CHAPTER ONE

1 INTROUDUCTION

In this section, the background and its significance of shrouded wind turbine discussed briefly. And also the scope, statement of the problem, methodology, objective and limitation of research discussed briefly.

1 .1Background and Significant of Study

The development and application of renewable, clean energy have become an important issue in recent years due to the serious effects of global warming and the rapid depletion of fossil fuels [1]. To report the current energy disaster various means of alternative energy are being examined. Wind energy technologies have become one of the fastest-growing energy sources in the world and it symbolizes a feasible alternative an effectively limitless resource. However, in comparison with the overall demand for energy, the scale of wind power usage is still very insufficient [2].

The large-scale conventional horizontal axis wind turbines are efficient and the modern megawatt wind turbines have a power coefficient of up to 40 % - 45 % [3]. However, they seek high wind speed to function a typically rated wind speed is about 12 m/s-14 m/s. Additionally, their installations are inadequate to regions far from the town due to some practical alarms related to safety risks and noise emission. In comparison, small scale wind turbines can work at low wind speed, generate minimal noise and there are no known safety risks. In spite of numerous advantages, very few small-scale wind turbine models have been developed. The currently available small to the mid-scale wind turbines mentioned in literature [4][5]. It is motivating to address that most of these wind turbines are in mid-scale range. The rated wind speed is characteristically above 10 m/s. None of the small-scale wind turbines excluding micro-wind turbines can function efficiently at the wind speed condition under 5 m/s. The micro-wind turbine which operates in a range of 2 m/s-7 m/s has an optimal power coefficient of 18 % which is pretty low. The current status of the small-scale wind turbines essentially highlights the lack of suitable its samples that can function near ground level at wind speeds of the instruction of a few meters per second.

The development of a new wind power system that can generate higher power output even in regions where lower wind speeds are prevailed would be cost-effective [3]. Also, in a conventional wind turbine, the wind flow is slowed down and expanded this phenomenon causes a loss in the efficiency of the turbine. Therefore, by generating a region of low pressure behind the turbine this used to reduce the corresponding loss.

In wind energy field the promising concepts is the development of wind power augmentation systems. So, a utilization of diffuser in the horizontal axis wind turbine system is also called as Diffuser Augmented Wind Turbine (DAWT). DAWTs were a burning issue at the 1979 wind energy innovative system conference. In DAWT the diffuser or flanged diffuser creates separation regions behind it, where low pressure fields develop to draw more wind through the rotors compared to a bare wind turbine.

Wind power generation in wind turbine is directly proportional to the cubic wind speed. Because of this a large increase in output of power is achieved if it is possible to increase in the velocity of the approaching wind flow to a wind turbine. It means that if we can increase the wind speed by flanged (or brim) diffuser the power output of a wind turbine can be increased significantly. In conventional horizontal axis wind turbine, the wind speed served from the location is directly used to generate power. But in shrouded wind turbine the available wind speed is increased by the diffuser to generate high power output. Currently very few researches have been informed the effect of diffuser shape in wind speed using computational simulations. [6, 7, 15]

The idea of diffuser is to increase the power output of a wind turbine by accelerating the wind velocity that approaches the wind turbine. To increase the wind velocity, a lower pressure would appear at the back of the wind turbine to act as a vacuum to suck the wind and accelerate it towards the blades. The region of areas surrounds or near the vortex would have typically lower pressure where the suction force will be formed by the vortex. Therefore, it will act as an accelerator to accelerate the wind velocity approaching the wind turbine. It was stated that vortex core will collapse the pressure field flow reversal and therefore no augmentation occurs [6]. This statement showed the alternative approach, where the vortex is used to generate a low-pressure region in the wake of the turbine. Vortex should appear at the wake of the diffuser but as little as possible inside the diffuser wall.

The acceleration of wind speed at the inlet of diffuser is the Couse of creation of low pressure inside a brim diffuser should not be less (or lower) than the pressure at the back of diffuser this can be obtained by minimizing separation of fluid flow on the inner diffuser wall and create as much vortices as possible at the back of flange of diffuser [7]

1.2 Scope of the study

This study focused on collecting and accelerating the wind energy to harness the wind for low wind speed region for this purpose in this study first step of this study investigates the effect of the shape of brim diffuser with different flange angles on velocity augmentation following this, based on the extension blade element momentum theory (EBEMT) theory. MATLAB code is developed to design the rotor blade of diffuser augmented wind turbine. After this, model the assemble drawing of shrouded wind turbine using a 3D CAD tool and analysis its performance in CFD fluent for a shrouded and bare wind turbine and lastly manufacture the model of shrouded wind turbine and model turbine was tested at the Addis Ababa Institute of Technology's laboratory to have a tangible confirmation of efficiency with the numerical result. The results obtained from both approaches (CFD and Experimental) were analyzed, compared and discussed.

1.3 Statement of the problems

To make the full usage of wind energy at low wind speed is a major difficulty in a conventional small-scale wind turbine because they are designed to have high power coefficient value at high wind speed and due to the addition of collecting accelerating device to blades the wind load and the weight of structure increase. Therefore, to reduce such kind of effect we need to investigate the optimum geometry of brim diffusers that shroud the wind turbine. In this research study the effect of the shape of the diffuser with different flange angles to obtain the optimum diffuser shape and flange angle and Conduct Numerical and experimental performance analysis of optimized DAWTs and compare with a bare small-scale wind turbine.

1.4 limitation of the research

The limitation of this research is the full designed size of the optimized diffuser augmented wind turbine is not tested in experiment because the size of the wind tunnel that found in thermal lab is not enough sufficent.

1.5 Objectives of the Research

1.5.1 Main Objective

The main objective of this research to study the effect of the shape of diffuser and flange angles on wind turbine diffuser performance and conduct numerical and experimental performance analysis of the optimized brim diffuser shrouded horizontal axis wind turbine to develop small type shrouded wind turbine for low wind speed regions.

1.5.2 Specific Objectives

- Sizing and Optimization of brim diffuse.
- Design of rotor blade for shrouded wind turbine.
- To determine and compare the performances analysis shrouded wind turbine and bare wind turbine by using CFD Fluent.
- Prototype manufacturing of shrouded wind turbine.
- Prototype experimental test and validation.

1.6 Research Methodology

The first step of this study investigates the effect of the shape of brim diffuser with different flange angles on velocity augmentation following this, based on the extension blade element momentum theory (EBEMT). MATLAB code is developed to design the rotor blade of diffuser augmented wind turbine. After this, model the assemble drawing of shrouded wind turbine using a 3D CAD tool and analysis its performance in CFD fluent for a shrouded and bare wind turbine and lastly manufacture the model of shrouded wind turbine and model turbine was tested at the Addis Ababa Institute of Technology's laboratory to have a tangible confirmation of efficiency with the numerical result. The results obtained from both approaches (CFD and Experimental) were analyzed, compared and discussed. A methodology is developed, as shown in Figure 1.1, to obtain objective.

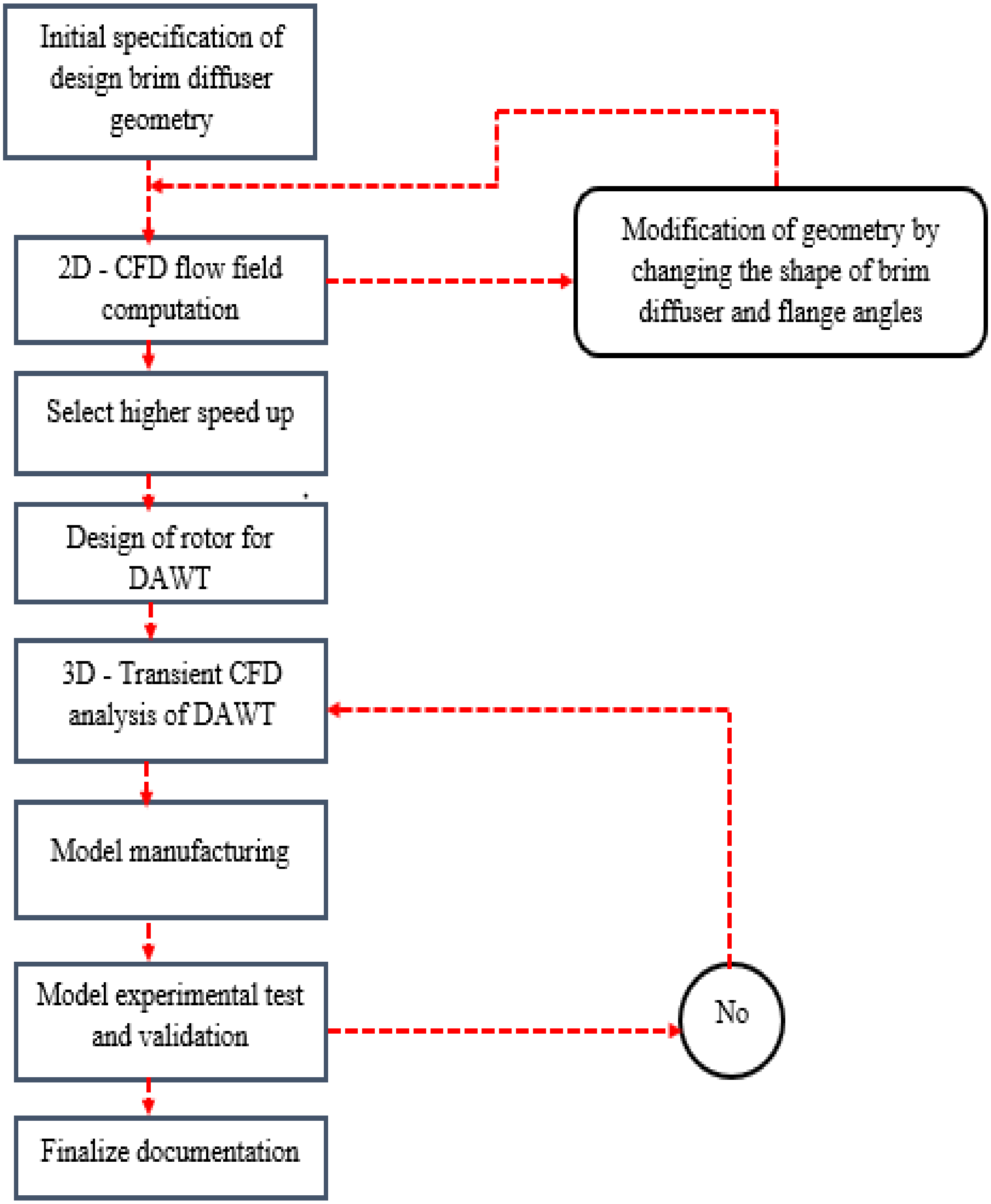

Figure 1.1 Research methodology chart

1.7 Research outline

This thesis is organized in seven chapters and the all chapters are organized as follows.

Chapter 1 describe a brief discussion of diffuser augmented wind turbine application. Function and its contribution for rural electrification for low wind speed region and the objective and the problem statement is presented in this chapter.

Chapter 2 a review of different research and its development of shrouded wind turbine were also presented.

Chapter 3 deals the geometry of brim diffuser by utilizing different optimization technique such as Sectional shape of diffusers and different diffuser flange's angles. The first one has a straight sectional shape with right angle inclination and the next two have curved sectional shape with different angles of inclination.

Chapter 4 deals the application of extended blade element momentum theory with diffuser on diffuser augmented wind turbine blade design and analyzing the aerodynamics performance of the rotor will be explained. A MATLAB code was developed to obtain chord and twist angle distributions in the presence of a diffuser was established.

Chapter 5 deals 3D transient numerical performance analysis of the optimized shrouded wind turbine and unshrouded wind turbine carried out, it is a catching device that can produce energy in the locations where small scale conventional horizontal axis wind turbines are too impractical to install and operate**.**

Chapter 6 describes the 3D Print or manufacturing and testing procedure for the diffuser augmented wind turbine model. Each component and its assembling drawing of DAWT using a 3D CAD tool solid work 2016. The brim diffuser manufacturing activities were carried out at local workshop and the rotor was printed with 3D printer machine found in Minister of Science and Technology and dynamo which were purchased from the local market.

Chapter 7 this chapter includes a summary of the critical relevant information of the research and recommendations for future work are also provided.

CHAPTER TWO

2 LITERATURE REVIEW

In this section a lot of researchers try to increase wind speed at a vicinity of wind turbine blades by different techniques. It is known that generated power by wind turbines is proportional to the cubic power of the approaching wind speed any small increase in the incident wind causes a large increase in the energy output. The shrouded or ducted wind turbine is one of the important used techniques to improve power captured. [14.15]

Ohya et al [8] Studied the effect of the shape of the duct such as nozzle, diffuser, and cylinder on the performance of a diffuser which accelerates the wind at the inlet of a diffuser. The experimental result shows that a diffuser ducted shape gives higher velocity augmentation when compared to other shapes of the duct. Also, he investigates the effect of the design parameter such as the brim length, hub ratio, and length of center body, open angle of a diffuser and addition of inlet shroud. Based on a numerical result the diffuser shaped duct with a flange at exit periphery of a diffuser and the presence of inlet shroud at the inlet of diffuser improve high velocity augmentation at the inlet of a diffuser.

Hansen et al. [9] conduct CFD simulation analysis to examine a diffuser augmented wind turbine which composed of NNACA 0015 airfoil around a bare wind turbine . Numerical result shows that the power coefficient for diffuser augmented wind turbine is proportional to the mass of wind flow that accelerated at the inlet of diffuser but the efficiency of diffuser is not studied.

Abe and Ohya [10] conduct a numerical and experimental investigation of flanged DAWTs. To develop small-type wind turbines below 1:5 kW. They conclude that the thrust coefficient for the best performance of a brim diffuser is considerably smaller than for a bare wind turbine. This is because the presence of brim at the exit of diffuser as shown in Figure 2.3 which create low pressure zone at the wake of diffuser because of the cruentation of vortex behind the brim. This reduction of low pressure draws more mas wind through the diffuse.

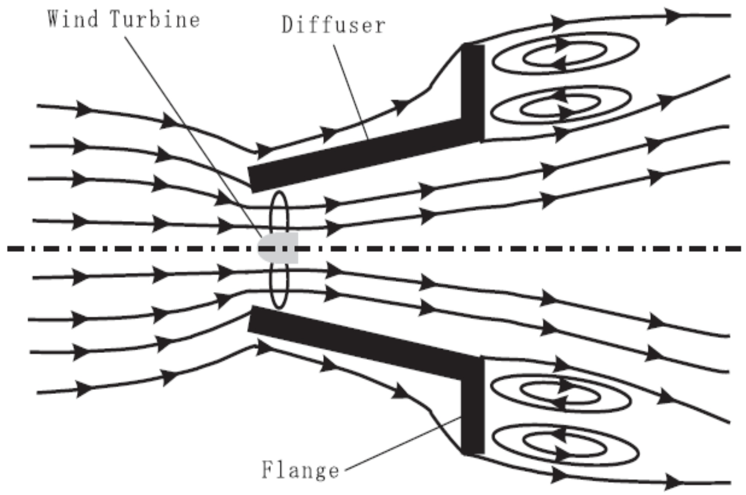

Figure 2.1 Schematic diagram of a wind turbine with a flanged diffuser showing the wind flow around the device (Abe & Ohya 2004)

Jafari and Kosasih [11] conduct CFD simulation analysis to study on small commercial wind turbine carried out with a simple frustum diffuser shrouding, which showed that augmentation is strongly dependent on the geometry of the diffuser, such as length and ratio of the diffuser outlet area to rotor area. The higher area ratio corresponds to high performance.

O. Igra et al [12] analyzed three different type of shrouded generation and conducted experimental work on wind tunnel. The first model was dropped due to high ratio length to diameter, which made it unsuitable for commercialization. The second model was a shortened version of the first nevertheless, the best outcomes obtained when the diffuser shaped look like an airfoil. Consequently, the third generate of shroud had an airfoil shaped diffuser so a prototype airfoil shaped diffuser built and monitored in a pilot plant. Compared BET with data Obtained from a shrouded wind turbine with a rotor diameter of 3 m and exit-area ratio of 1.6 producing 0.75 kW at 5 m/s with a power augmentation ratio (over the bare turbine) of 2.4.

Kosasih and Hudin [13] examined the performance of a unshrouded wind turbine and shrouded micro wind turbine models subject to different levels of turbulence. It was shown that the diffuser increases the power coefficient by a factor of almost two. Beyond a certain tip-speed ratio, the performance of both unshrouded and shrouded wind turbine decreased with increasing turbulence intensity, however the power coefficient of the shrouded wind turbine was still greater than that of the unshrouded wind turbine indicating the diffuser augmentation was still achievable even at high turbulence.

Lubitz and Shomer [14] investigate the practicality of the shrouded turbine relative to the unshrouded horizontal axis wind turbine and analyze the importance of determine the benefits of a diffuser against the addition of costs and the diffuser also contains a benefit of review of the history of shrouded turbine.

Sørensen and Hansen [15] showed that the increasing wind flow through the rotor placed in a diffuser correspond a directly proportional to the force that acting on the diffuser. They determine the thrust force-based om momentum theory and conclude that it is dependent only that back pressure that formed at the wake of diffuser

Gilbert and Foreman [16] introduce 1D a semi - empirical theory applied to shrouded turbine and focus on concentrating and accelerating wind energy in a diffuser with a high open angle, a boundary layer flow separation controlled with slots adopted to understand a flow that goes along the inside surface of the diffuser. This method of boundary layer control avoids pressure loss by flow separation and enhance the mass flow inside the diffuser.

Bet and Grassmann [17] developed a shrouded wind turbine with the addition of a wing ring structure at the exit of diffuser. It concludes that the shrouded wind turbine showed an enhance the power output by the wing system by a factor of 2.0 compared to unshrouded wind turbine.

Fletcher et al [18] introduce an extended blade element momentum theory to shrouded wind turbine by including wake rotation, blade Reynolds number effects, the diffuser efficiency, and area ratio, but diffuser thrust and far-wake velocity were not considered.

Anzai et al [19] conducted experimental analyses for the introduction of a concentrator as shown in Figure2.2) around a turbine, and the design specification of the object is shown in Figure 2.2. The first the rotor was positioned behind the outlet of concentrator the concentrator must be placed 50 mm to 150 mm before the turbine rotor and the second the concentrator outlet diameter must be slightly smaller than the rotor diameter and the concentrator inlet diameter must be much larger than the turbine. The result show that approximately 25% increase on the power coefficient when compared to a unshrouded wind turbine.

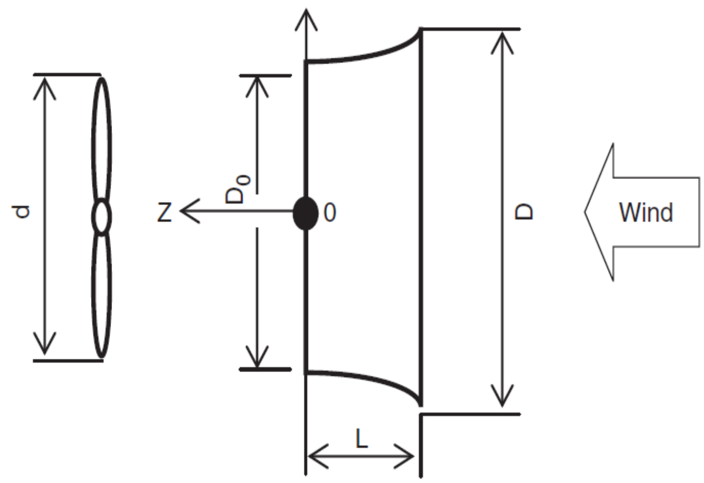

Figure 2.2 Sketch of concentrator and wind turbine (Anzai et al 2004)

Harrington and Caitlin [20] introduce an advanced method to the analysis of shrouded horizontal axis wind turbine using the Blade Element Momentum, Computational Fluid Dynamics design on diffusers and conservation principles. The results for the estimated diffuser velocity speed-up ratio agree with the experimental data and same behavior is gained for the torque and the output power when compared to the numerical and experimental outcomes existing from the literatures.

J. Vaz and D. Wood [21] introduced a new performance analysis of a shrouded wind turbine taking into account the influence of the diffuser efficiency and thrust force, in which a new construction for the far-wake velocity is proposed and also algorithm to assess shrouded wind turbine and the performance was developed and implemented the new model was validated by comparison with experimental data.

As mentioned in literature the velocity augmentation strongly dependent on diffuser geometry parameters such as length of the flange, length of diffuser, area ratio and the opening angle of a diffuser. The effect of such a parameter on velocity and power augmentation is more studied by other researchers [1, 2, 3, 4, 5, and 6]. However, the effect of sectional shape of brim diffuser with different flange angle on wind turbine diffuser performance is not studied before therefore in this paper study the effect of shape of brim diffuser with different flange angles on velocity and power augmentation and conduct the performance analysis of the optimized diffuser augmented wind turbines (DAWTs) is analyzed by using ANSYS- FLUET to develop small type diffuser augmented wind for low wind speed regions. This will allow the use of wind power in applications in remote areas of Ethiopia and around Ethiopia where low wind speeds prevail.

CHAPTER THREE

3 OPTIMIZATION OF BRIM DIFFUSER

In this section was determining an optimum geometry of brim diffuser by utilizing different optimization technique such as Sectional shape of diffusers and different diffuser flange's angles, due to this, made two types of diffuser with different sectional shape and flange angle as shown in Figure 3.1 and also the geometry of each model is tabulated in Table 3.1. The first one has a straight sectional shape with right angle inclination and the next two have curved sectional shape with different angles of inclination. Flange angles of these tested samples vary from -20^0 to 20^0 . This section also describes assumptions and methods used for CFD analysis and optimization of brim diffuser by using ANSYS Fluent software.

The optimization parameters of the brim diffuser are

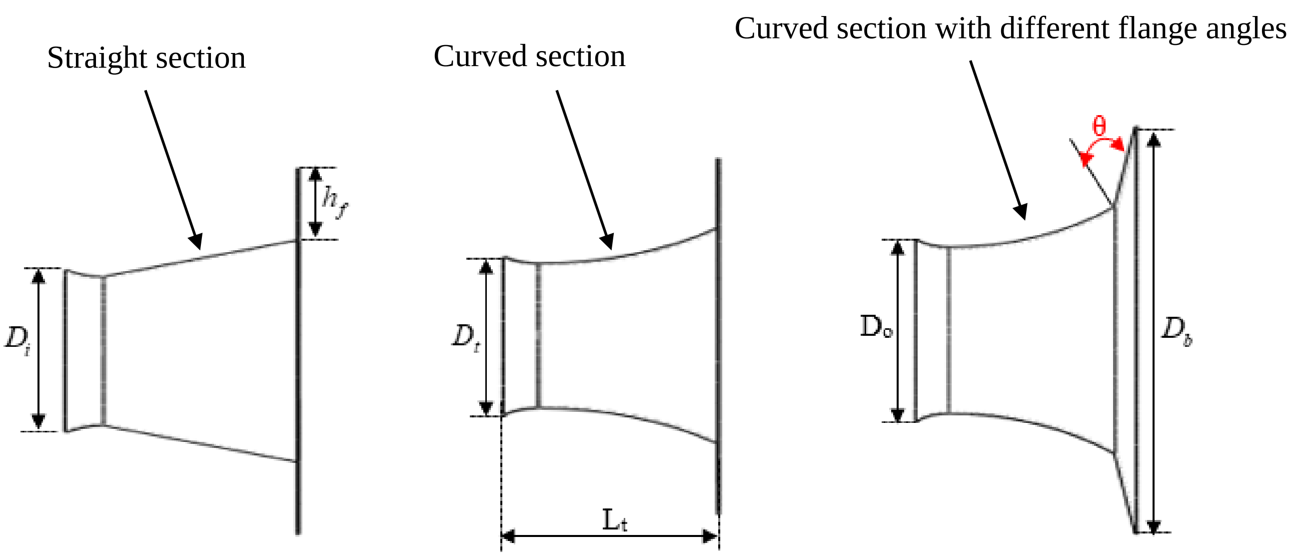

Figure 3.1 Variation of Sectional shape and inclination of flange angles for brim diffuser

Table 3.1 The geometry of each model

Sectional shape of brim diffuser	Throat diameter D_t	Rotor diameter D_r	Area ratio A_o/A_i	Length ratio L_t/D_t	Brim height h_f	Angel of brim with horizontal line	Inlet shroud length L_{shroud}
Curved	0.52	0.5	2.35	1.03	$0.5\,D_{throat}$	90^0	0.8
Straight	0.52	0.5	2.35	1.03	$0.5\,D_{throat}$	90^0	0.8
Curved with different flange angel	0.52	0.5	2.35	1.03	$0.5\,D_{throat}$	-20^0 to 20^0	0.8

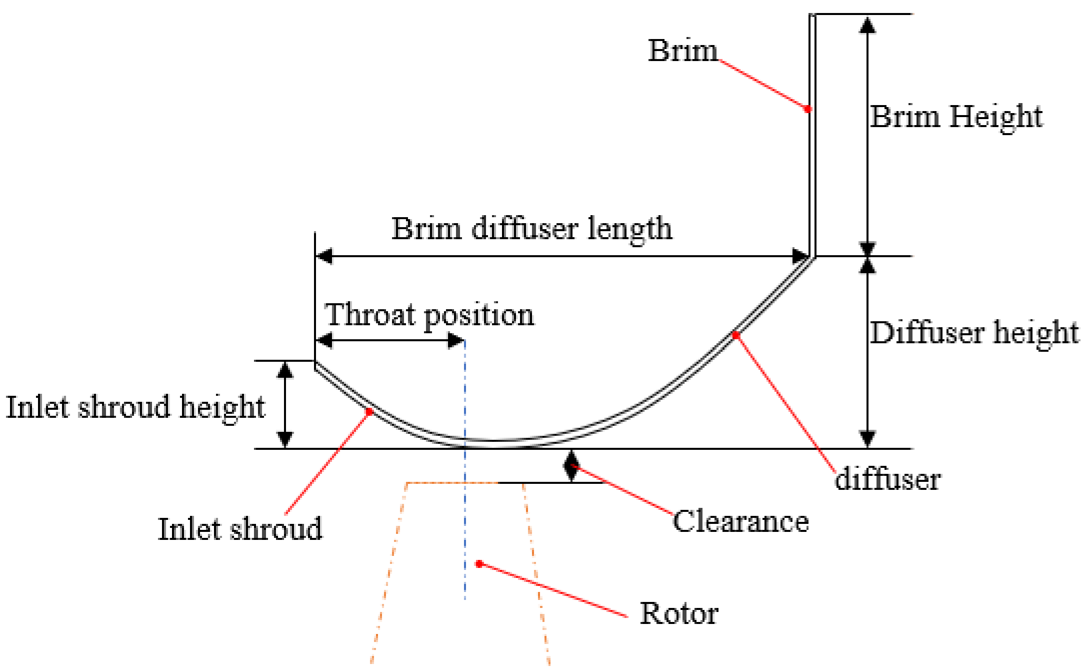

Figure 3.2 Design parameters for diffuser augmented wind turbine (DAWT)

3.1 Governing equations

The governing equation of the computational domain is viscous flow that describe three fundamental principles of conservation: Conservation of mass (continuity), Conservation of momentum (Newton's 2nd law) and Conservation of Energy (1st law of thermodynamics). Equations 3.1, 3.2 and 3.3 represent Navier Stokes equations of conservation of mass, momentum and energy respectively. The fluid used is incompressible and there is not significant change in temperature. Equations 3.4 and 3.5 are the modification for incompressible fluid and by neglecting energy equation.

$$\frac{\partial(\rho)}{\partial t} + \rho \nabla V = 0 \qquad 3.1$$

$$\rho \frac{dV}{dt} = \rho g + \nabla.\tau_{ij} - \nabla P \qquad 3.2$$

$$\rho \frac{dV}{dt} = \rho g + \nabla\left(k\nabla^2 T\right) + \phi \qquad 3.3$$

$$\nabla.V = 0 \qquad 3.4$$

$$\rho \frac{dV}{dt} = \rho g + \mu \nabla^2 V - \nabla p \qquad 3.5$$

The governing equations are a coupled system of non-linear partial differential equations. Due to the non-linear partial differential governing equation of the flow filed difficult to solve the exact solution of the governing equation but it can be solving numerically by numerical software. There are many commercially available codes (CFX, Fluent, STAR-CD, etc.) where a solution can be calculated. The numerical analysis of CFD in diffuser consists of incompressible fluid flow. In addition, the temperature effect is negligible during the analysis. Therefore, conservation of energy is ignored during analysis.

Due to lack of supercomputer and to reduce, computational cost. Approximations would have to be made Based on this the flow is assumed as steady, incompressible .2D analysis and axisymmetric due to symmetric nature of brim diffuser. Similar method can be found in [10,22,23]

3.2 Computational condition and boundary condition

Due to symmetrical nature of the configuration of the brim diffuser as shown in Figure 1, the flow considers two-dimensional. [10]The present computational conditions [22] and grid system around a flanged diffuser are shown in Figure 2, 3 respectively.

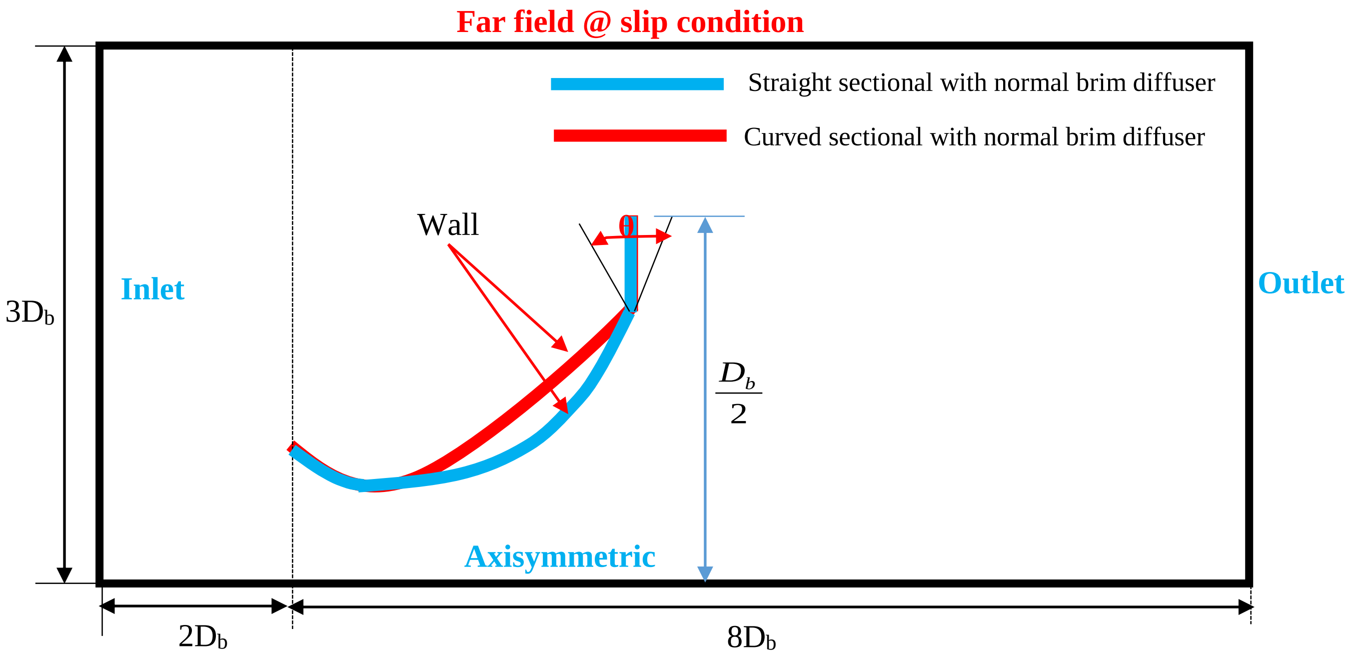

Figure 3.3 Computational domain and bounders applied on the domain of Half Axisymmetric sectional shape of the candidate brim diffusers

3.3 Meshing

The problem domain discretization is achieved by dividing the domain boundaries into a finite number of nodes to create a finite number of cells. This discretization by using global and local meshing method using edge sizing, inflation method. The generated mesh is shown in Figure 3.3 and extremely more element was created on the brim diffuser surface, which is shown in closed up view of Figure 3.3 with inflation layer to account the turbulence effect at the wall.

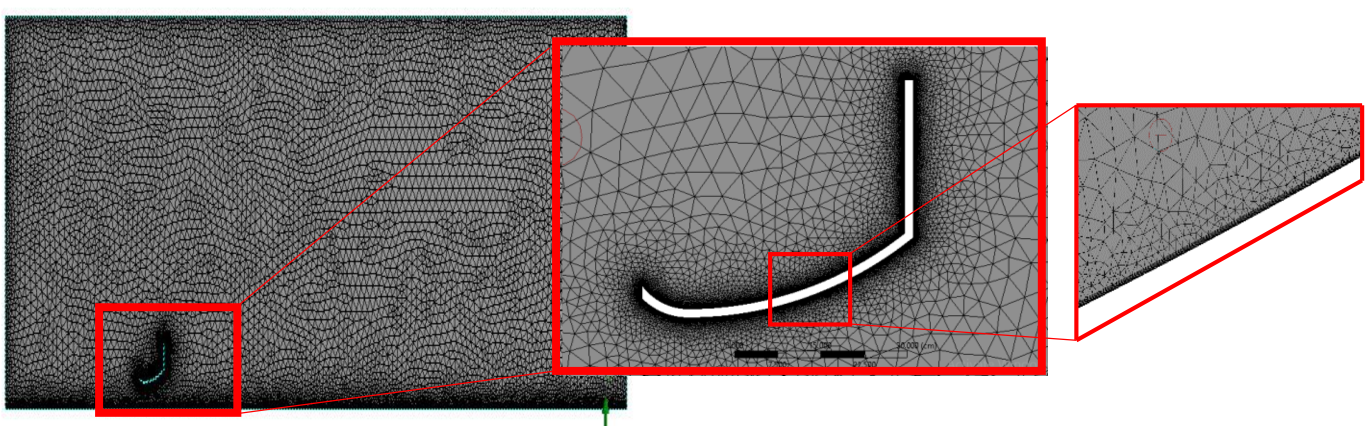

Figure 3.4: Meshed computational domain (left) closed up view of mesh around brim diffuser (right): sizing and inflations applied

Two important metrics determine the quality of a mesh. In other words, how a mesh element's proximity or departure does from a mathematically defined shape is dictated by the mesh, metric. Two of the most important mesh metrics are (a) Orthogonal quality and (b) Skewness Orthogonal quality has a maximum value of 1 and minimum value of 0, Skewness has to be close to zero. Skewness equaling 1 is deemed as inferior quality mesh. Here we can see from graph the most of element have in the range of [0.15-1] and skewness [0.95 - 0] which is in the acceptable range [24]

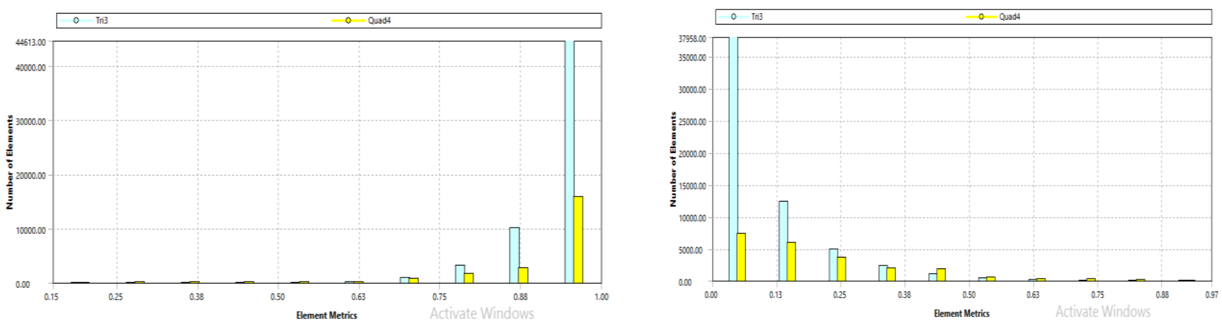

Figure 3.5 Mesh metrics: orthogonal quality (left) skewness (right)

3.4 CFD fluent Setup

The flow field is modeled by the continuity and incompressible Navier –Stokes equations and the turbulent model is transition SST Turbulence model based on the recommended flow Reynold number. In the analysis of turbulent flow, the y+ values are in the range of 0.00187 to 0.3797, which is the acceptable range for transition SST Turbulence model (y+ < 1) [25] and first-order numerical scheme is used to compute the convection and diffusion terms [26]. A uniform and steady flow is set at the inlet boundary, no-slip boundary condition is specified on the surface (wall) of the flanged diffuser and zero-pressure condition is prescribed at the outlet boundary, slip boundary condition is applied to the top boundary, and axisymmetric condition is applied to the bottom boundary (the axisymmetric axis) similar methods can be found in [10] . The inlet boundary condition, a uniform flow with 5% of free stream turbulence was specified [26]. Iterative CFD analyses are performed using a CFD code of ANSYS Fluent 18, which is a useful CFD code for modeling fluid flow in complex geometry

3.5 Grid Independency Test

Grid convergence used to describe the improvement of result by using successively smaller cell size for the calculation; the calculation should approach the correct answer as mesh become finer. It means that computing the solution on successive finer grid. Figure 3.5 demonstrates how the results change with a greater number of cells. It is quite clear that the mesh created in the analysis (which has around 75,329 cells) is fine enough to obtain a sufficiently accurate solution

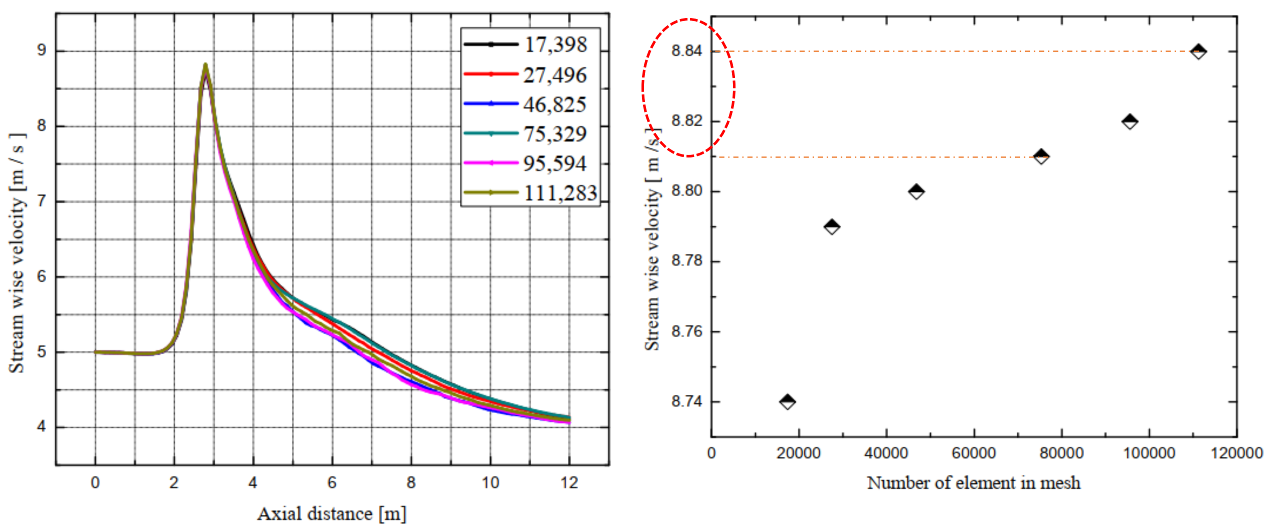

Figure 3.6 Streamwise velocity distribution of brim diffuser for different mesh size (left) maximum stream wise velocity for different mesh size (right)

Because a small change (0.028) in the velocity speed - up ratio from an approximately two-fold increase in a number of elements in the mesh and Convergence of the numerical solution is represented by a negligible change in velocity speed - up ratio from an approximately five-fold increase in a number of elements in the mesh. The mesh was refined by adjusting global and local mesh controls: relevance center, face sizing, and inflation. To obtain a mesh of 111,283 elements (right-most data point in the plot), the relevance center was set to fine; the face size was set to 0.05m; for inflation, the number of layers was to 10 at a growth rate of 1.2.

Therefore, grid convergence analysis has been carried out by monitoring velocity speed up ratio as a parameter of significant interest. This is done in order to get a solution that does not vary significantly even when we refine our mesh further.

3.6 Model Verification

This model is verified with experimental results that were done by Ohya et al. [27]. The geometry of diffuser that is done by experiment is inlet dimeter $D_{in} = 12cm$, outside diameter $D_{out} = 24cm$, area ratio 4 and angle of inclination (φ) is 3.714^0 the length ratio $\left(L/D = 7.7 \right)$. The diffuser geometry is shown in Figure 3.7.

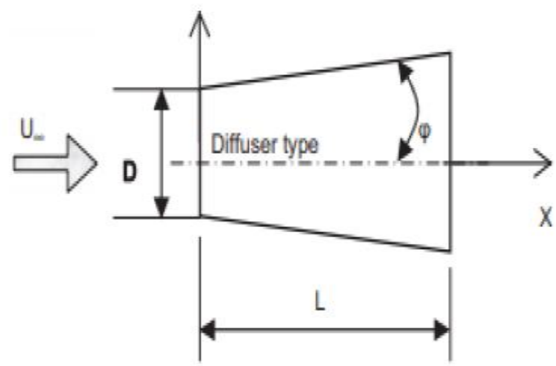

Figure 3.7 Diffuser geometry

In numerical analysis a diffuser duct is set with the same diffuser geometry under same condition to ohya experiment. From Figure 3.7 shows axial velocity distribution at centerline of diffuser for both cases. The difference between the two curves that is shown in Figure. Varies from 0.3% to 5.3%. These values show a good agreement between present numerical method by CFD fluent and Ohya's experimental results.

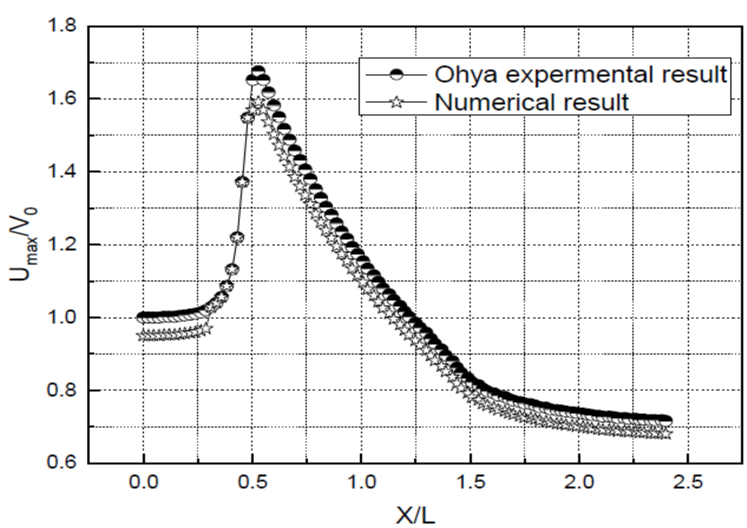

Figure 3.7 Ohya's experimental and numerical results

3.7 Result and Discussion

Numerical modeling gives a detail information the flow filed inside and outside a brim diffuser this used to analysis the effect of the design parameter on the diffuser performance as shown below.

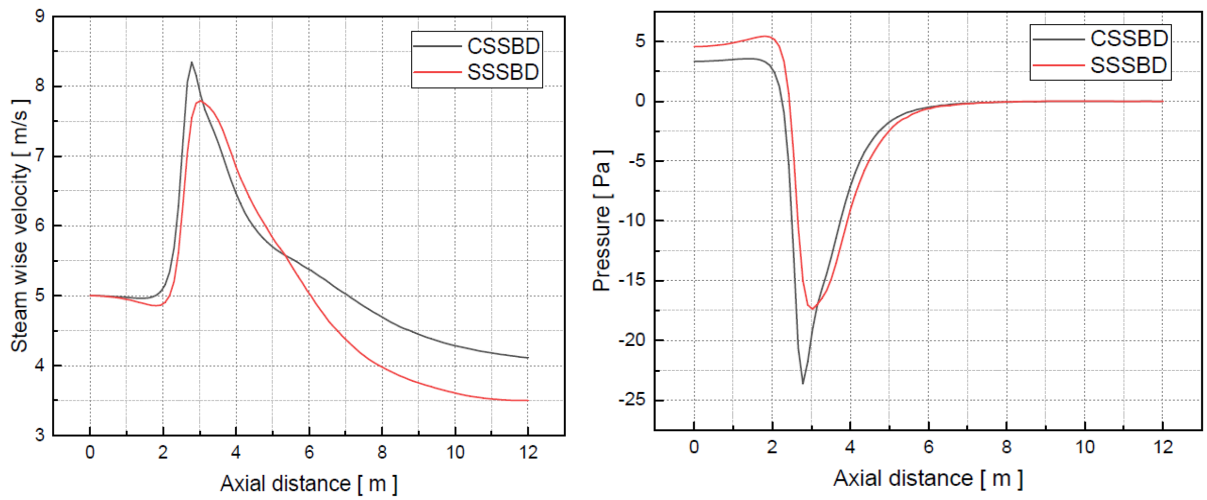

Figure 3.7 Streamwise velocity distributions on the central axis of a brim diffuser (right) ad Static pressure distributions (left) for both sectional type

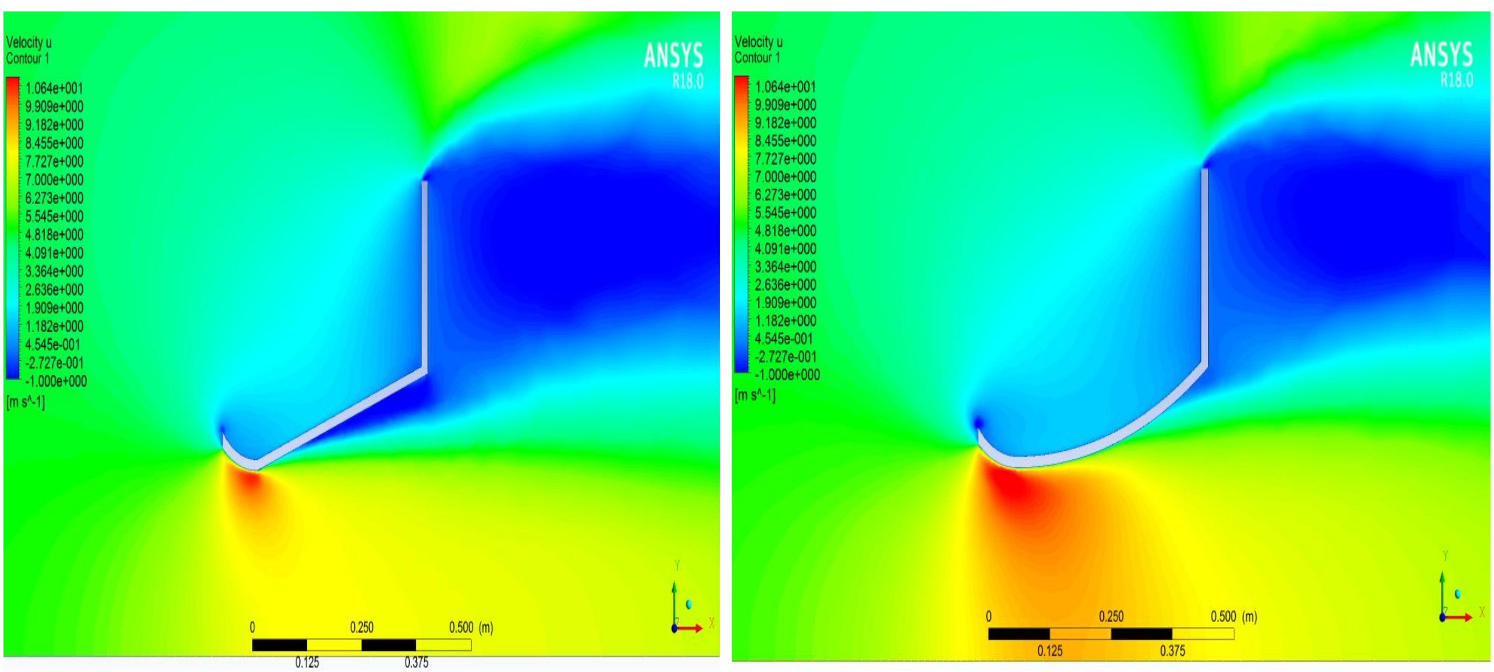

Figure 3.8 Velocity distributions in straight sectional shape (left) and curved sectional shape (right) brim diffuser

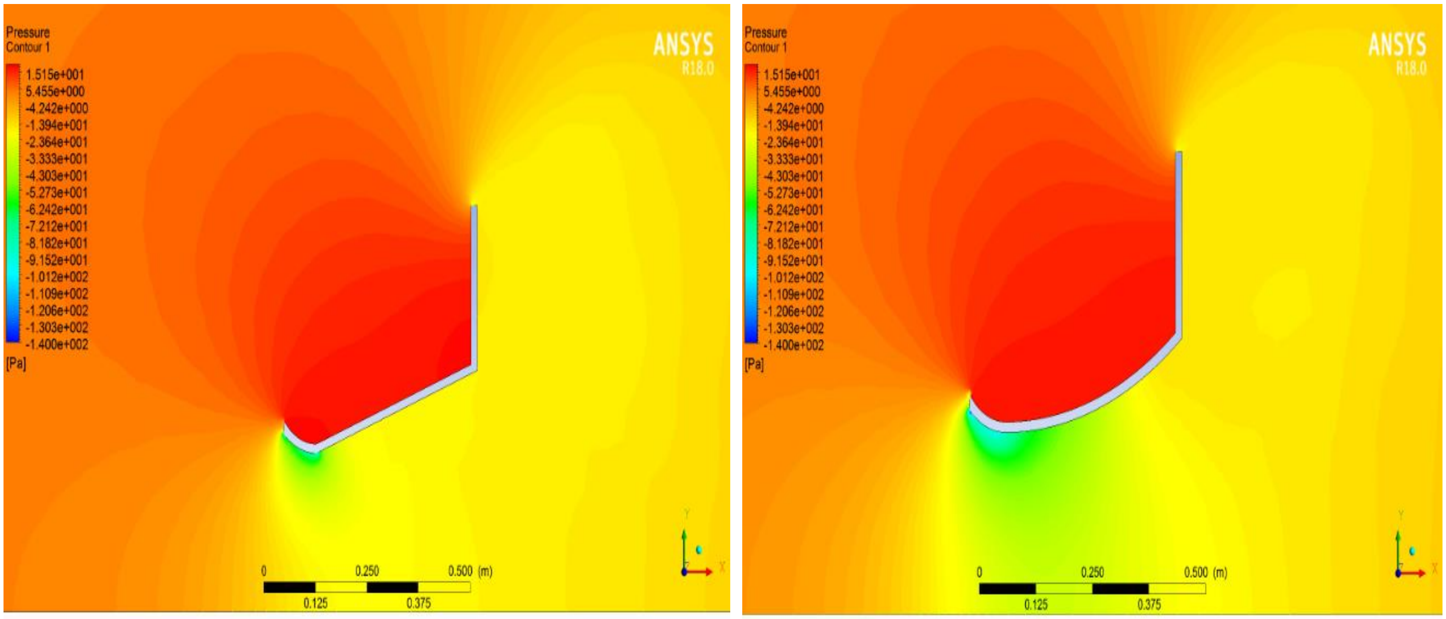

Figure 3.9 Pressure distributions in straight sectional shape (left) and curved sectional shape (right) brim diffuser

Figure 3.7 to 3.9 clearly shows the acceleration mechanism of approaching flow can be understood. When air flow inside and outside of brim diffuser the wind velocity is accelerated at the entrance of diffuser this is because of the creation of low pressure at the wake of diffuser which act as vacuum to suck wind and accelerate it. The main reason for the creation of low pressure is the role shape of diffuser and brim (or flange), the role of brim is to make vortex at the back of flange this cause creates low pressure and draw more wind into a diffuser.

In this comparison, Figure 3.8 to 3.9 it can be seen that the curve sectional shape of the brim diffuser induces a larger region of lower pressure inside the diffuser, which corresponds to higher velocity and better performance. Figure 3.7 shows that the curved sectional shape of brim diffuser increases the velocity at the inlet of the diffuser from $V_0 = 5m/s$ to $V_{\max} = 8.34m/s$ but in straight section reach to $V_{\max} = 7.79m/s$. Therefore 7.06 % velocity augmentation is achieved in the curved shape of diffuser than a straight diffuser. The main reason for this is the boundary-layer flow along the inside wall of the curved diffuser does not show a large flow separation. Figure 3.10 shows that in curved brim diffuser the starting point of flow separation arises at 40cm from the inlet of brim diffuser, which is a point where the wall shear stress vanishes, but in straight sectional shape of brim diffuser it starts to separate at 22 cm. Which shows that nature of the flow separation points inside of a diffuser greatly affect the acceleration of airflow through a diffuser. Therefore, the velocity augmentation and reduction of the size of a flanged diffuser is very important in the development of small and middle scale horizontal axis wind turbine shrouded by a flanged diffuser.

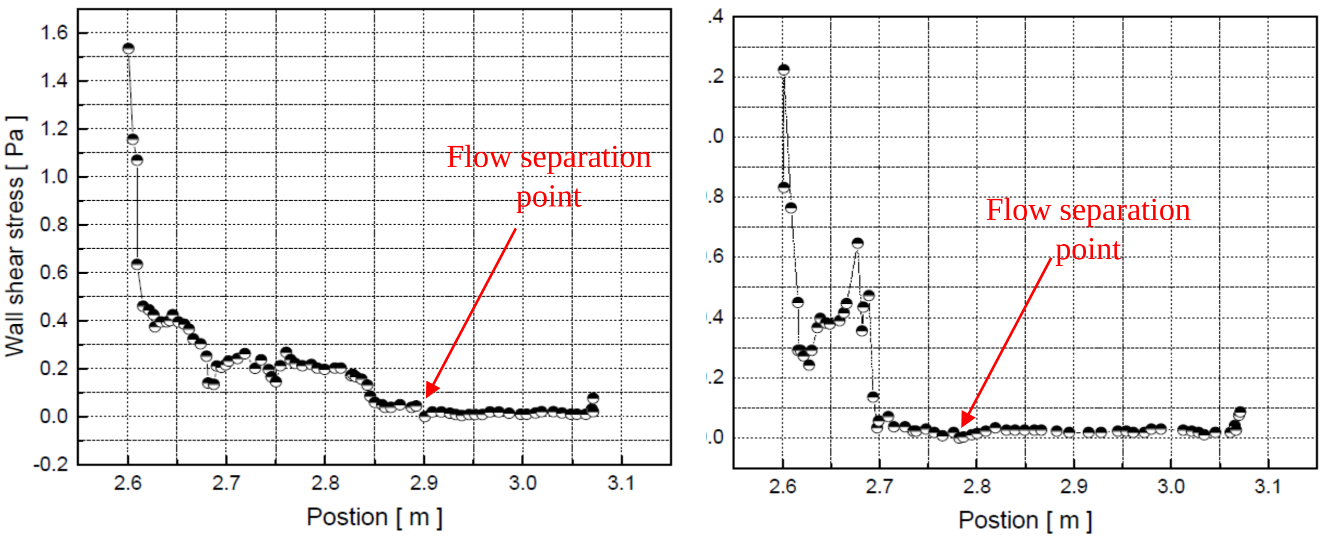

Figure 3.10 Flow separation point in boundary layer flow along inside of a brim diffuser for curved sectional shape of brim diffuser (left), straight sectional shape of brim diffuser(right)

In addition, we investigate the effect of flange's angles for the curved sectional shape of a diffuser as a varied parameter on velocity increment at diffuser entrance. All samples have the same sectional shape of brim diffuser and have the same dimension of shroud length, entrance diameter, exit diameter, and flange length but

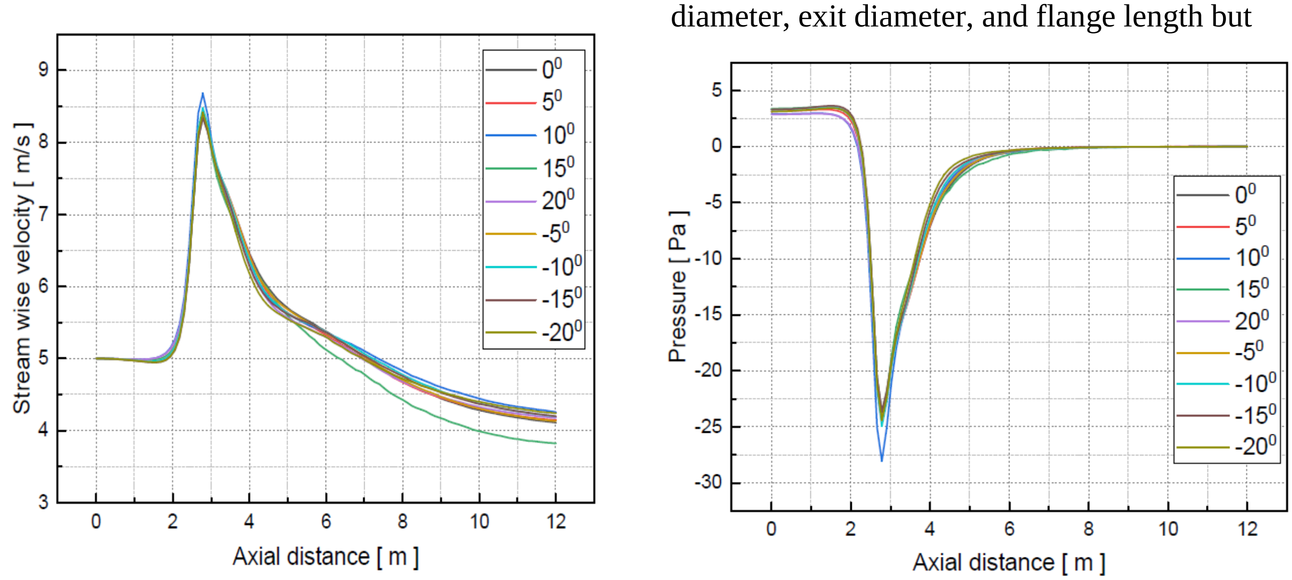

Figure.3.11 Relation of stream wise velocity distribution at diffuser entrance (left) and pressure distribution (right) for different flange angles.

the only difference is flange angles. Which vary from -20^0 to 20^0 . The numerical result from Figure 3.11 shows that the $+10^0$ optimum flange angles that accelerate the wind speed at the entrance of diffuser from the candidate flange angles. The main reason for this is the centration of strong vortices behind a flange this Couse or induce large low pressure at the wake of diffuser to suck more wind at the entrance of diffuser.

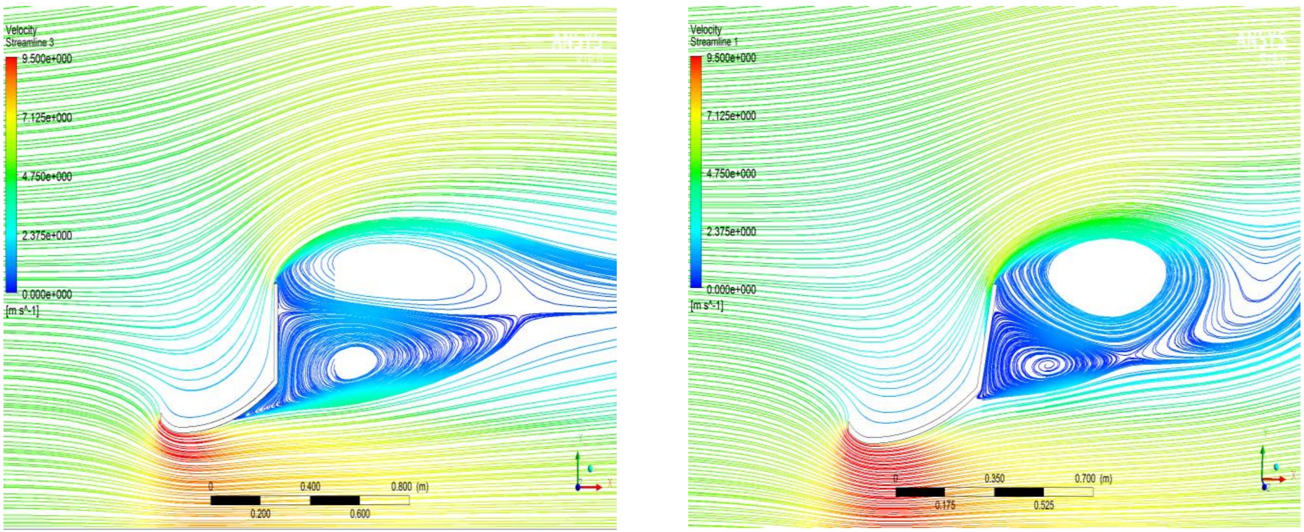

Figure 3.12 stream line velocity distribution and vortices behind the flange for 0^0 (left) and 10^0 (right) flange angles

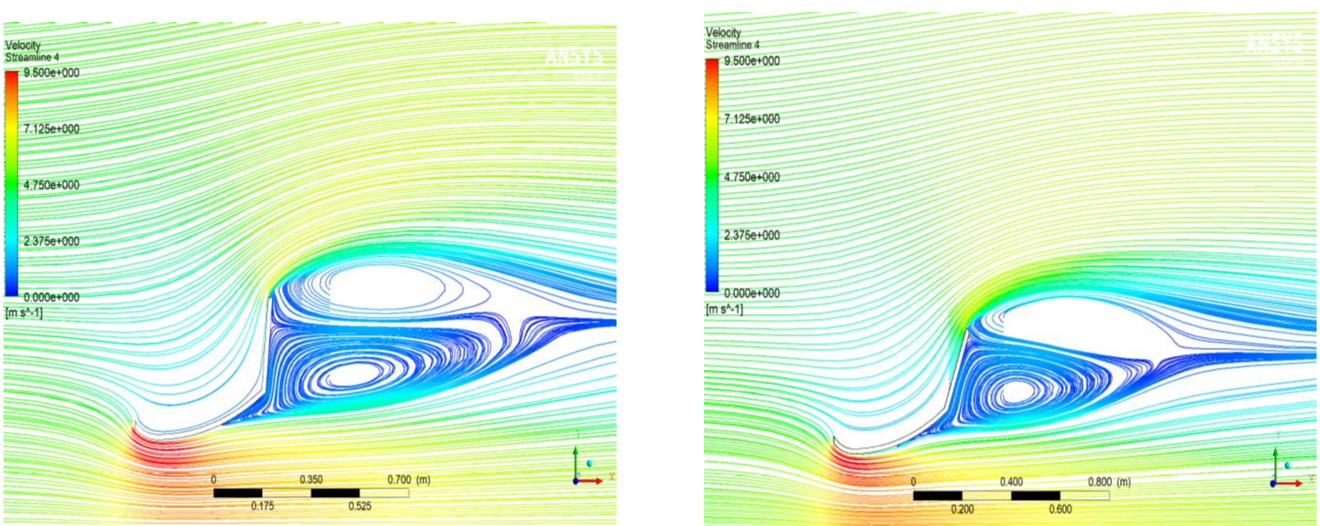

Figure 3.13 stream line velocity distribution and vortices behind the flange for 5^0 (left) and 20^0 (right) flange angles

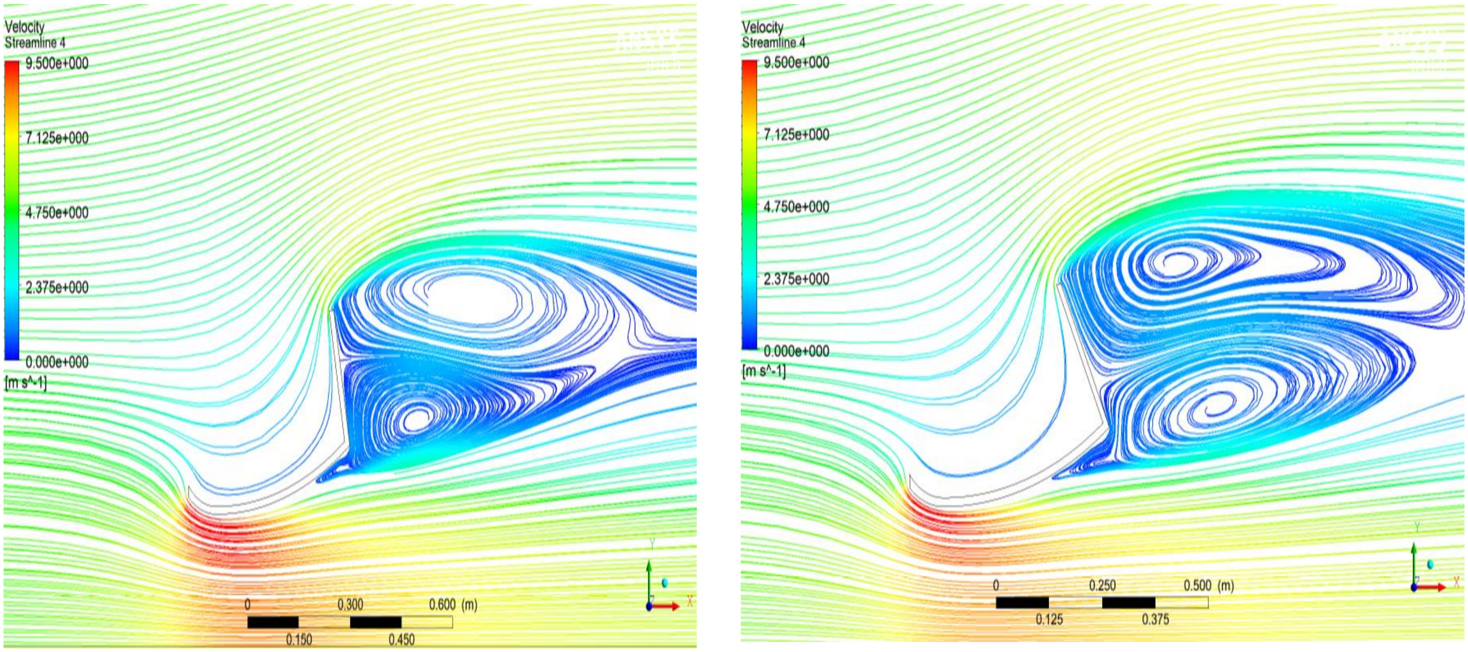

Figure 3.14 stream line velocity distribution and vortices behind the flange for -10^0 (left) and -20^0 (right) flange angles

From Figure 3.12 and Figure 3.13 to 3.14 clearly show that at $\theta = 10^0$ the velocity reaches a value of $8.68m/s$ at diffuser entrance, which gives higher velocity augmentation by 4 % when compared to other flange angles This is because of the magnitude of the created vortices at $\theta = 10^0$ is relatively higher than other case, this causes high pressure drop behind the flange of brim diffuser which increase the mass flow rate and velocity at diffuser entrance.

CHAPTER FOUR

4 DESIGN OF ROTOR BLADE FOR DAWT

In this section, the application of extended blade element momentum theory with diffuser on diffuser augmented wind turbine blade design and analyzing the aerodynamics performance of the rotor will be explained. A MATLAB code was developed to obtain chord and twist angle distributions in the presence of a diffuser was established. The concept of tip loss factor and the introduction to airfoil selection criteria in DAWT blade design will be discussed.

4.1 The classical actuator disk model theory with diffuser

To describe the classical actuator disk model theory with diffuser a similar formulation is used as classic theory but considering losses through the diffuser [28]. Figure 4.1 shows the control volume for the actuator disc with diffuser [21]

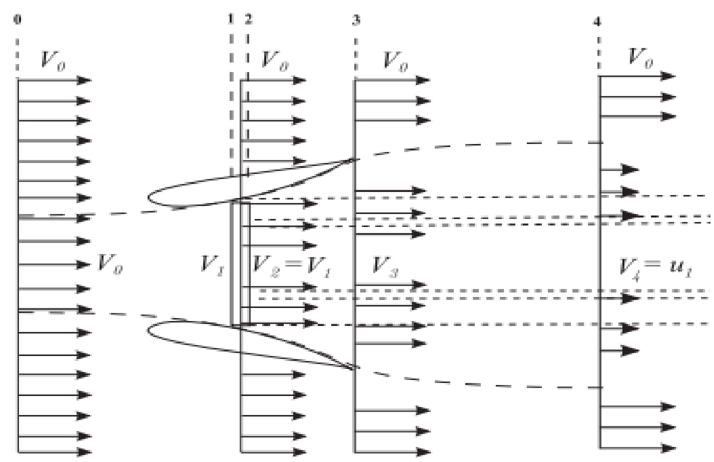

Figure 4.1 Velocities at the rotor plane and in the wake [29]

The power coefficient, C_p for the classical theory with diffuser is given by [30]

$$C_p = \varepsilon\left[1-\left(\frac{V_4}{V_0}\right)^2-(1-\eta_d)(1-\beta^2)\varepsilon^2\right] \tag{4.1}$$

Applying the energy balance downstream to the diffuser exit gives the relationship for the velocity V_4

$$\left(\frac{V_4}{V_0} = \beta^2 \varepsilon^2 + c_{p3}\right) \tag{4.2}$$

Substituting Eq. (4.2) in Eq. (4.1), yield

$$C_p = \varepsilon\left(1 - c_{p3}\right) + \varepsilon^3\left[\eta_d\left(1 - \beta^2\right) - 1\right]$$

It is assumed that $V_4 = \left(1 - 2a\right)V_0$ where a is the conventional induction factor at the rotor and the same condition for the axial velocity in the wake of an ideal bare wind turbine is applied in the flow after the diffuser outlet. The diffuser speed-up ratio, γ is defined as the ratio between the maximum axial flow velocity in the diffuser and the free stream velocity. Thus, the velocity approaching the disc becomes $V_1 = V_2 = \gamma\left(1 - a\right)V_0$ and $\varepsilon = \gamma\left(1 - a\right)$

Eq. (4.3) give

$$C_p = \gamma\left(1 - a\right)^2\left[4a + \gamma^2\left(1 - a\right)\left(1 - \beta^2\right)\left(\eta_d - 1\right)\right] \tag{4.4}$$

If no losses occur in the diffuser ($\eta_d = 1$), Equation (4.4) results in

$$C_p = \gamma 4a\left(1 - a\right)^2 \tag{4.5}$$

The Bernoulli equation can be used in the two control volumes on either side of the actuator disk. Between the free-stream and upwind side of the rotor (from section 0 to 1 in Figure 4.1) and between the downwind side of the rotor and far wake (from section 2 to 4 in Figure 4.1) respectively

$$\Delta p = p_2 - p_1 = \frac{\rho\left(V_1^2 - V_4^2\right)}{2} \tag{4.6}$$

The thrust can also be expressed as the net sum forces on each side of the on the ring on the rotor annuli of $dA_2 = 2\pi r dr$

$$dT = \Delta P x dA_2 = \frac{\rho\left(V_1^2 - V_4^2\right)}{2} dA_2 \tag{4.7}$$

We know that the velocity at the rotor plane and in the wake $V_1 = V_0(1-a)$, $V_4 = V_0(1-2a)$ respectively

Eq. 4.7 gives

$$dT = \rho V_1^2 4a(1-a)\pi r dr \tag{4.8}$$

And the power produced by the annular ring will be

$dp = dTxV_2$ Since $V_2 = \gamma V_0(1-a)$

$$dp = \gamma\rho V_1^3 4a(1-a)^2 \pi r dr \tag{4.9}$$

The thrust coefficient will be

$$dC_t = \frac{dT}{\frac{1}{2}\rho(2\pi r dr)V_0^2} = 4a(1-a) \tag{4.10}$$

And the power extraction will be

$$c_p = \frac{dp}{\frac{\rho(2\pi r dr)V_0^3}{2}} = \frac{\gamma\rho V_0^3 4a(1-a)^2 \pi r dr}{\frac{\rho(2\pi r dr)V_0^3}{2}} = \gamma 4a(1-a)^2 \tag{4.11}$$

4.2 Effect of rotation

The previous analysis can be extended to the case where the rotating rotor generates angular momentum which can be related to rotor torque. In the case of a rotating wind turbine rotor the flow behind the rotor rotates in the opposite direction to the rotor in reaction to the torque exerted by the flow on the rotor. The generation of rotational kinetic energy in the wake results in less energy extraction by the rotor than would be expected without wake rotation.

If it is assumed that the angular velocity imparted to the flow stream (ω) is small compared to the angular velocity (**Ω**) of the wind turbine rotor then it can also be assumed that the pressure in the far wake is equal to the pressure in the free stream [31] The analysis that follows is based on the use of an annular stream tube with a radius r and a thickness dr

In this analysis the rotor disk is divided into many concentric annular rings and calculate the torque and the power of the entire disk can be obtained by integrating through annular rings dq is obtained directly from the angular momentum equation applied to an infinitesimal control volume of area [32] $dA = 2\pi rdr$

To derive an expression for the torque on the rotor by applying the conservation of angular momentum. For this situation the torque exerted on the rotor q must equal the change in angular momentum of the wake on an incremental annular area element this gives

$$dq = d\dot{m}\omega r^2 \tag{4.12}$$

Since $d\dot{m} = \rho V_2 dA = \rho V_2 \left(2\pi rdr\right)$,$V_2 = \gamma\left(1-a\right)V_0$ and $\omega = a'\left(2\Omega\right)$ Equ.3.12 reduce to

$$dq = 4\rho a'\gamma\left(1-a\right)V_0\Omega r^3 dr \tag{4.13}$$

The power generated at each element dP is given by

$$dP = \Omega dq \tag{4.14}$$

Substituting Eq.3.13 in Eq.3.14 and using the definition of the local speed ratio which is $\lambda_r = \Omega r / V_0$ the expression for the power generated at each element becomes

$$dP = \frac{1}{2}\gamma\rho A_2 V_0^3\left[\frac{8}{\lambda^2}a'\left(1-a\right)\lambda_r^3 d\lambda_r\right] \tag{4.15}$$

It can be seen that the power from any annular ring is a function of the axial and angular induction factors and the tip speed ratio. The axial and angular induction factors determine the magnitude and direction of the air flow at the rotor plane. The local speed ratio is a function of the tip speed ratio and radius.

The incremental contribution to the power coefficient, dC_p from each annular ring is given by

$dC_p = \dfrac{dp}{1/2\rho dAV_0^3}$ thus gives

$$C_p = \frac{8}{\lambda^2}\int_0^{\lambda} \gamma a'(1-a)\lambda_r^{\,3} d\lambda_r \quad (4.16)$$

4.3 Blade element theory with a diffuser

The above two theory restrict the understanding of the effect of rotor geometry (i.e. blade airfoil section, chord and twist). The blade-element theory is an alternative method of analyzing the behavior of blades due to their motion through air

As shown in Figure 4.2 for this analysis, it is assumed that the blade is divided into N sections (or elements) and the aerodynamic force acting on each blade element can be estimated as the force on suitable airfoil characteristics of the same cross-section adopted for the blade elements. Finally, assuming that the behavior of each element is not affected by the adjacent elements of the same blade, the force on the whole blade can be derived by adding the contributions of all the elements along the blade [33]

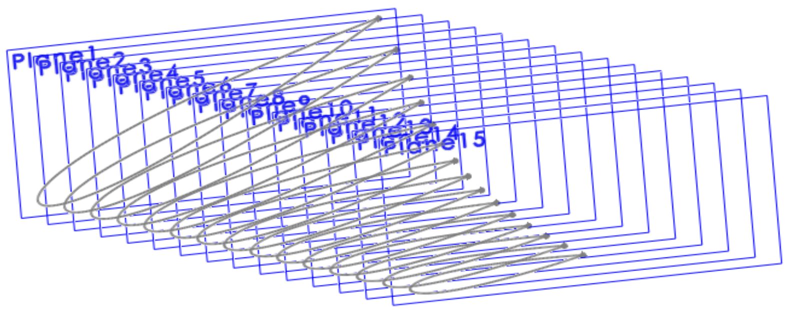

Figure 4.2 Schematic of blade elements

A diagram showing the developed blade element at radius r and the velocities and forces acting on this element is given in Figure 4.3

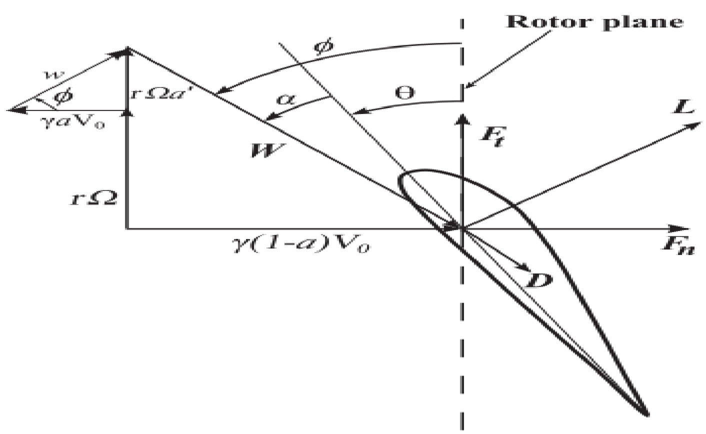

Figure 4.3 Blade geometry for analysis of a DAWTs [23]

From the velocity diagram in Figure 4.3 the following relationships can be determined

$$\tan\varphi = \gamma \frac{(1-a)V_0}{(1+a')\Omega r}$$

$$\varphi = \phi + \alpha \qquad (4.18)$$

$$W = U_{rel} = \frac{V_0(1-a)}{\sin\phi} \qquad (4.19)$$

As we know Lift and drag coefficient of airfoil are defined as

$$C_l = \frac{L}{1/2\rho U_{rel}{}^2 c} \qquad (4.20)$$

$$C_d = \frac{D}{1/2\rho U_{rel}{}^2 c} \qquad (4.21)$$

From this the drag and lift force for a given airfoil will be

$$dF_l = 1/2 C_l U_{rel}{}^2 cdr \qquad (4.22)$$

$$dF_d = 1/2 C_d U_{rel}{}^2 cdr \qquad (4.23)$$

The normal and tangential force coefficient will be

$$dF_n = dF_L \cos\phi + dF_d \sin\phi \qquad (4.24)$$

$$dF_t = dF_L \sin\phi - dF_d \cos\phi \qquad (4.25)$$

In this section the diffuser is incorporated into BET by using the control volume shown in Figure 4.1. The induced velocities, v_1 and v_2 , shown in Figure 4.1 are given by $\gamma(1-a)V_0$ while the flow velocity at the diffuser outlet, V 3, using the continuity equation, can be written as

$$V_3 = \beta V_1 = \beta\gamma(1-a)V_0 \qquad (4.26)$$

And the normal and tangential force coefficient will be

$$C_n = \frac{F_n}{1/2\rho W^2 c} = C_l \cos\phi + C_d \sin\phi \qquad (4.27)$$

$$C_t = \frac{F_t}{1/2\rho W^2 c} = C_l \sin\varphi - C_d \cos\varphi \qquad (4.28)$$

Therefore, the rotor has B number of blades the total normal (trust) and tangential force on the element at a distance r by rearranging Equation 4.24 and 4.25 with the use of equation 4.17 and 3.19

$$dF_n = 1/2B\rho U_{rel}{}^2 cdr(c_l \cos\phi + c_d \sin\phi) \qquad (4.29)$$

$$dF_t = BrdF_t = 1/2B\rho U_{rel}{}^2 cdr(c_l \sin\phi - c_d \cos\phi) \qquad (4.30)$$

The elemental torque due to the tangential forces dF_t operating at a distance r from the center is given by

$$dq = rdF_t \qquad (4.31)$$

Hence the elemental torque by inserting equation 4.30 into equation 4.31

$$dq = 1/2B\rho U_{rel}{}^2 crdr(c_l \sin\phi - c_d \cos\phi) \qquad (4.32)$$

Inserting Equations 4.29 and Equations 4.30 in equation 4.32 the general form of elemental thrust and torque equations become

$$dF_n = \sigma\pi\rho \frac{V_0{}^2 (1-a)^2}{\sin^2\phi}(c_l \cos\phi + c_d \sin\phi) \qquad (4.33)$$

$$dq = \sigma\pi\rho \frac{V_0{}^2 (1-a)^2}{\sin^2\phi}(c_l \sin\phi - c_d \cos\phi) r^2 dr \qquad (4.34)$$

From blade element theory two Equations (4.33 and 4.34) have been obtained. They define the normal force (thrust) and the tangential force (torque) on an annular rotor section as a function of the flow angles at the blades and airfoil characteristics

4.4 Blade Element-momentum (BEM) Theory with diffuser

BEM theory refers to the determination of a wind turbine blade performance by combining the equations of general momentum theory and blade element theory with diffuser. In this case by equating the elemental thrust force equations from general momentum theory and blade element theory (Equations 4.32 and 4.33 respectively) the following relationship is obtained

$$\frac{a}{1-a}=\frac{\gamma^2 Bcc_n}{8\pi r\sin^2\phi} \qquad (4.35)$$

$$\frac{a}{1+a'}=\frac{Bcc_t}{8\pi r\sin\phi\cos\phi} \qquad (4.36)$$

4.5 Tip loss factor

There was an assumption the rotor has an infinite number of blades which was used in all theories with the aid of this assumption radial velocity of the flow across the rotor plane and in the wake has been always neglected and by so the derivations of governing equations have been established but near the boundary of the slipstream the air tends to flow around the edges of the blade tips and acquires an important radial velocity. Because the pressure on the suction side of a blade is lower than on the pressure side which causes the air to flow around the tip.

Clifon-Smith [29] observe two important observations to be made for DAWTs. First, the diffuser is assumed to induce a circumferentially uniform axial flow but no azimuthal flow through the rotor. This axial flow should reduce the tip loss, as should the proximity of the blade tip to the diffuser wall, in a way that is not possible to incorporate F (tip loss factor) into BEMT with diffuser. Second, there should be different tip loss factors for the axial and circumferential motion

4.6 Optimization model for DAWTs

To maximize power extraction the maximize will be obtained every possible value of $\lambda_r\gamma a'(1-a)$ is maximize based on Equation 4.16

$$C_p=\frac{8}{\lambda^2}\int_0^{\lambda}\gamma a'(1-a)\lambda_r^{\,3}d\lambda_r$$

In order to integrate this expression one needs to relate the variables a, a' and λ_r to express a' in terms of a. Consider pressure drop across the rotor from actuator disk model and rotary actuator disk model the local tip speed ratio will be

$$\frac{\lambda_r^2}{\gamma^2} = \frac{a(1-a)}{a'(1+a')} \tag{4.37}$$

$$a' = -\frac{1}{2} + \frac{1}{2}\sqrt{\left[1 + \frac{4a(1-a)}{\lambda_r^2}\right]} \tag{4.38}$$

The aerodynamic conditions for the maximum possible power production occur when the term $\gamma a'(1-a)$ in Equation (4.16) is at its greatest value. Substituting the value for a' from Equation 4.38 into $\gamma a'(1-a)$ and setting the derivative with respect to a equal to zero yields

$$\gamma^2 \lambda_r^2 = \frac{(1-a)(4a-1)^2}{(1-3a)} \tag{4.39}$$

This equation defines the axial induction factor for maximum power as a function of the local tip speed ratio in each annular ring. Substituting into Equation (4.37) one finds that, for maximum power in each annular ring a' will be

$$a' = \frac{1-3a}{4a-1} \tag{4.40}$$

4.7 Airfoil selection

4.7.1 Flow Reynolds number estimation

The density and dynamic viscosity of air at room temperature is $\rho = 1.204 kg/m^3, \mu = 1.516x10^{-5} m^2/s @ 20^0 c$ respectively. The lift over drag ratio of an airfoil decreases drastically with decrease in flow Reynolds number [34]. Therefore, the flow Reynolds number is the first and foremost step of the design process. Reynolds number can be calculated using

$$\mathrm{Re} = \frac{\rho c U_{rel}}{\mu} \tag{4.41}$$

It's important to notice that the expression contains relative wind speed and not the absolute wind speed. Relative wind speed can be calculated using

$$U_{rel} = \sqrt{\left[(1-a)V_0^{\,2}\right]^2 + \left[(1+a')\Omega r\right]^2} \tag{4.42}$$

Also, there are many variables whose values are not known at the beginning, such as induction factors and rotation rate ω and the chord length. Each of these variables needs to be wisely guessed. Assume induction factors and equals to zero Rotation rate ω can be calculated using

$$\lambda = \frac{\Omega r}{V_\infty} \tag{4.43}$$

But tip speed ratio λ is unknown. As the application is to generate electricity, prefer a low solidity rotor with minimum number of blades and working at high tip speed ratio. For aerodynamic and structural stability, a three bladed rotor is considered.

We know that Number of blades in a rotor is directly related to the design tip speed ratio. The higher the tip speed ratio, the lower would be the number of blades [32]. Figure 4.4 gives a guideline for choosing the number of blades based on the design tip speed ratio.

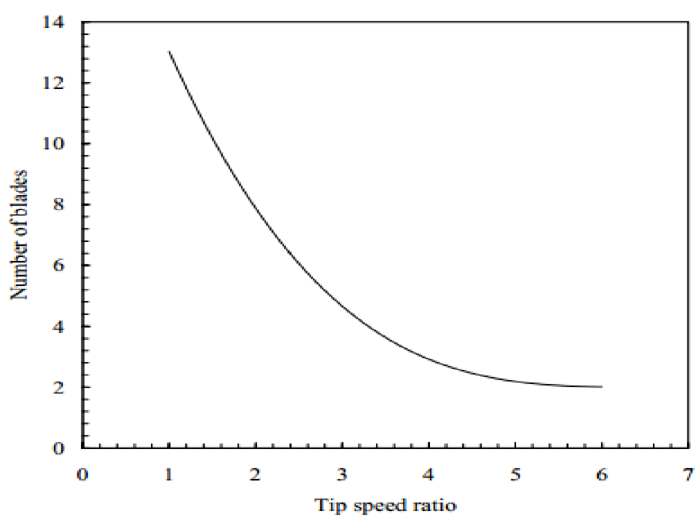

Figure 4.4 Number of blades vs tip speed ratio [32]

From Figure 4.4, it is logical to take a design tip speed ratio of $\lambda = 6$ for such rotors. Based on equation (4.43) give $\Omega = 63.33 \, {rad}/{\sec}$ Assume average chord length should be estimated by considering the structural rigidity which is 15% of the diameter of wind turbine [35] $c_{avg} = 15\% D_r = 0.27m$

For a wind turbine having diameter of 180 cm and tip speed ratio of 6, the Reynolds number based on equation 4.41 can be calculated to be 1.2 x 10^6

Once the flow Reynolds number has been estimated, the next step was to determine an appropriate airfoil, which performs well at the given Reynolds number. After study of many literatures, it has been concluded that S835 is the airfoil design for application of wind turbine has been gives more useful to other airfoil [36]

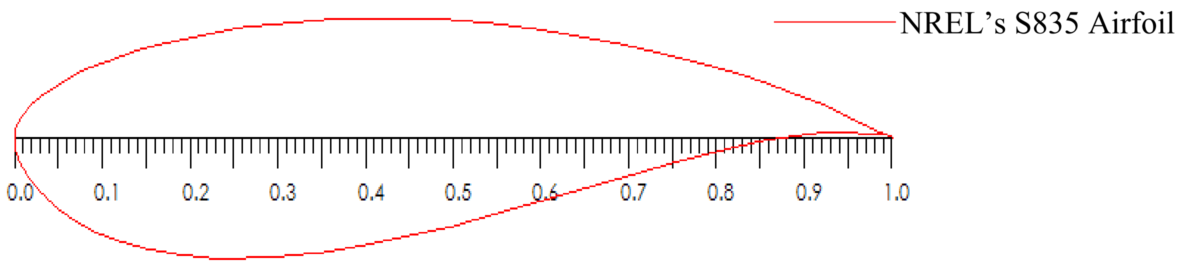

Figure 4.5 shape of NREL's S835 Airfoil

Figure 5 shows the lift and drag coefficients (C_l and C_d) and glide ratio (${C_l}/{C_d}$) of S835 at Reynolds number Re= 1.2 x 10^6 obtained using program Q- **Blade-XFLR 5v6.06** . An analysis tool for the airfoils 1.2 x 10^6 Reynolds number. S835 airfoil has maximum lift over drag ratio at 93 at the angle of attack $\alpha = 4^0$

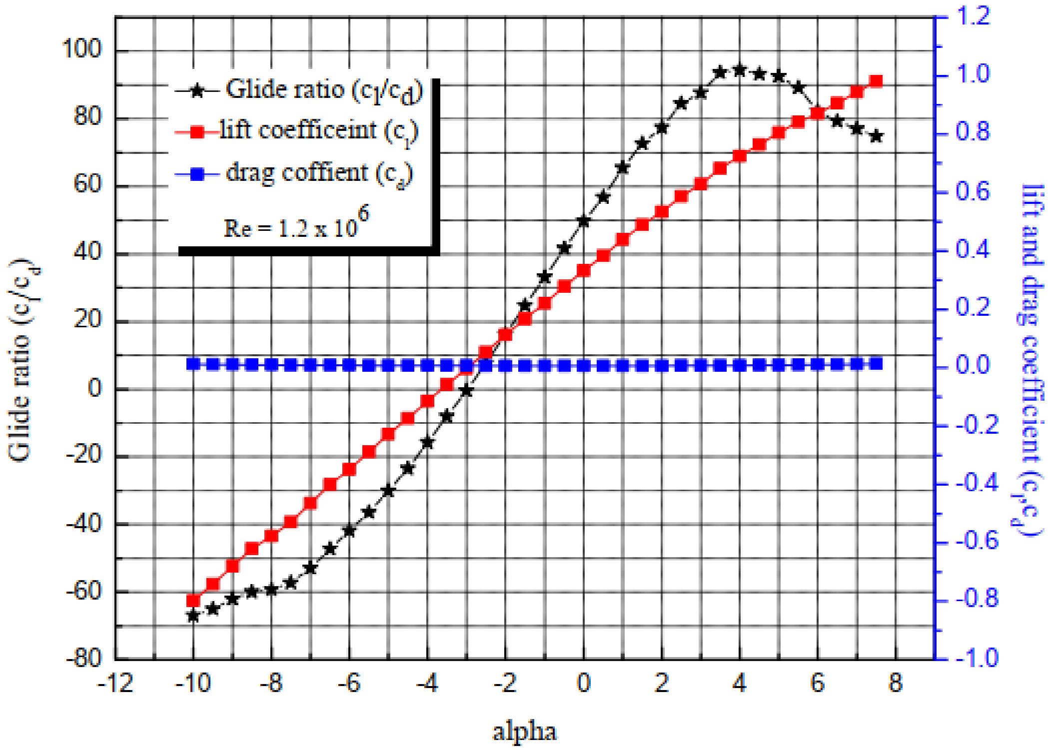

Figure 4.6 Characteristics of S835 airfoil at Re 1.2 x 10^6

The design lift and drag coefficient @ 4^0 angle of attack $C_l = 0.725$ and $C_d = 0.00768$ respectively. Therefore, from figure 4.6 the design lift and drag coefficient @ 4^0 angle of attack is $C_l = 0.725$ and $C_d = 0.00768$ respectively.

4.8 Algorithm to design the blade of the rotor for DAWTs

A MATLAB code was developed to obtain chord and twist angle distributions in the presence of a diffuser was established. as shown below. Iterative scheme (Algorithm to develop chord and twist distribution along blade) the calculation of optimum chord and twist angle is not so straight forward. It requires an iterative procedure to calculate the values of induction factors for each of the elements. The main steps of the iterative method used in this study are as following

a) Divide the blades into n numbers of span-wise elements.
b) Start with some guess values of a and a' (initial guess, $a = 1/3$ and $a' = 0$)
c) Calculate relative inflow angle using Equations (4.17) for all the elements

d) Calculate normal and tangential force coefficient using (Equations 4.27 & 4.28) for all element
e) Compute the optimum values for a using Equations (4.40)
f) Compute the optimum values for a' using Equations (4.38)
g) Compute the optimum chord distribution using equation 4.35 for all blade elements
h) Compute the optimum twist distribution using equation 4.18 for all blade elements
i) Compute the new value for relative inflow angle using Equations (4.17)
j) If inductions factors change more than a certain tolerance. Go to step b or else finish
k) Compute the chord and twist distribution on the segment of the blade

From the above algorithm. A MATLAB code was developed to obtain chord and twist angle distributions in the presence of a diffuser was established. and it's MATLA CODE is show in **appendix B.** Which gives Twist angle and chord distribution of the rotor of the blade are show in Figure 4.7

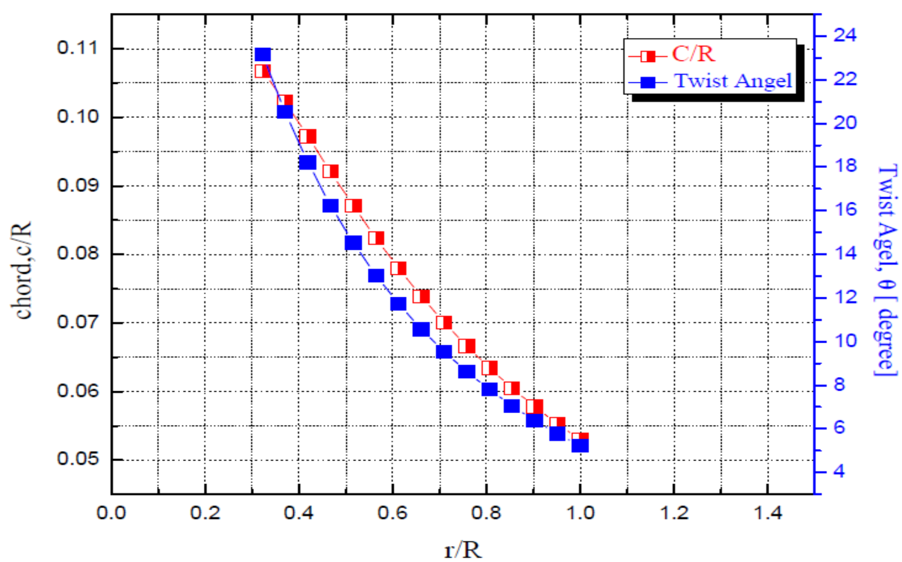

Figure 4.7 Chord and twist angle distributions as a function of the radial position

CHAPTER FIVE

5 THE PERFORMANCE ANALYSIS OF BRIM DIFFUSER SHROUDED HORIZONTAL AXIS WIND TURBINE BY CFD FLUENT

In this section, 3D transient numerical performance analysis of the optimized shrouded wind turbine and unshrouded wind turbine carried out, it is a catching device that can produce energy in the locations where small scale conventional horizontal axis wind turbines are too impractical to install and operate. The main objective of the present section is to determine the maximum torque that is generated from the optimized diffuser augmented wind turbine (DAWTs) as designed in chapter 3 and 4. In addition, we demonstrate the performance of a scaled model of DAWTs by using CFD analysis to validate with experimental result.

5.1 Computational domain

This section describes the method and modeling used for conducting 3D CFD simulation of diffuser augmented wind turbine. Figure 5.1 shows the completed CAD drawing of rotating and stationery domain, which is model separately and assembled. Stationary domain contains a brim diffuser and cylinder to accommodate an interface between the two domains and rotating domain contains turbine of rotor and rotating cylinder for interface purpose.

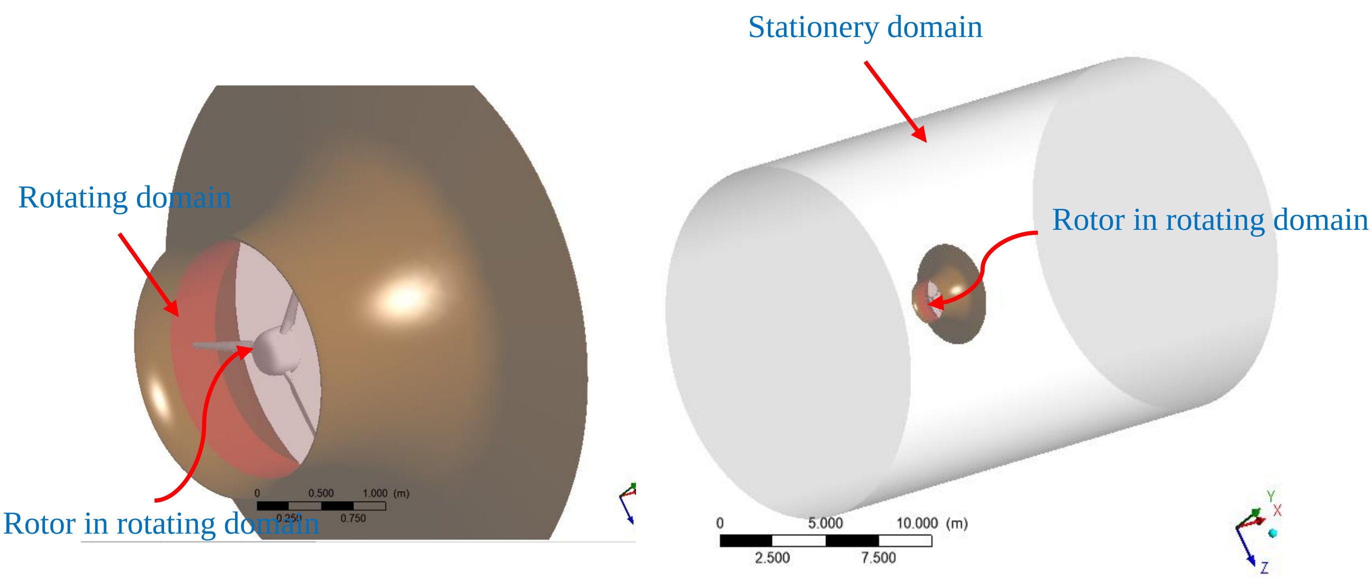

Figure 5.1 Assembling of the Rotating and Stationery domain (right) and closed up view brim diffuse with rotor (left)

5.2 Discretization

The problem domain discretization is achieved by dividing the domain boundaries into a finite number of nodes to create a finite number of cells. This discretization is made by using global, local meshing method and using edge sizing, inflation method. The generated mesh is shown Figure 5.2 both stationary and rotating domains meshed as they are imported into CFD Fluent.

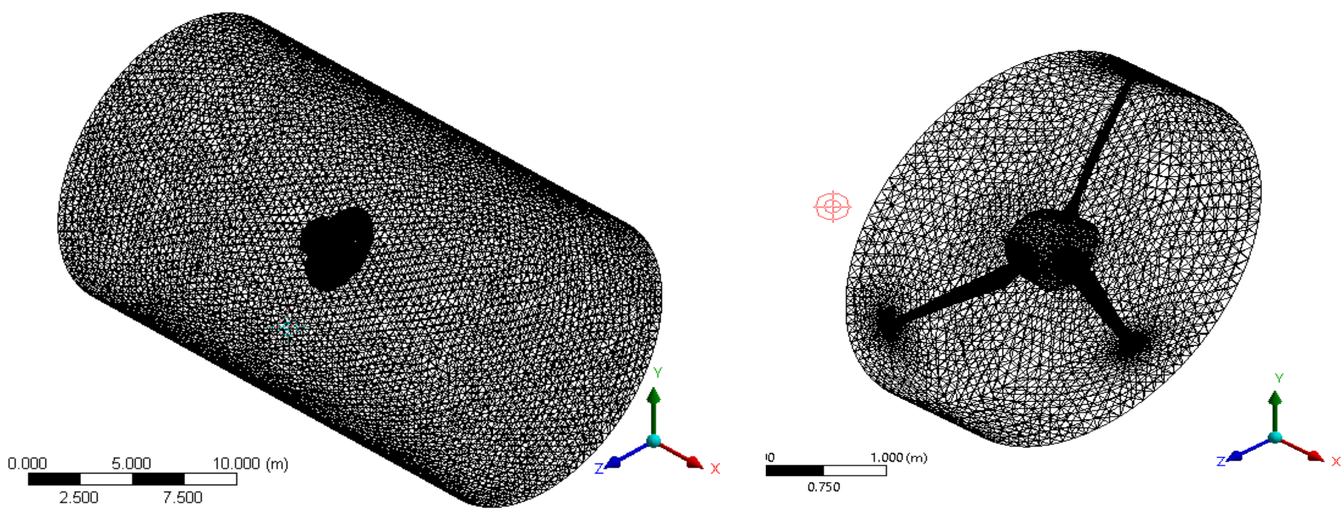

Figure 5.2: Meshed Rotating (right) and Stationary domain (left): sizing and inflations applied

There are two important metrics that determine the quality of a mesh. In other words, how a mesh element's proximity or departure does from a mathematically defined shape is dictated by the mesh, metric. Two of the most important mesh metrics are (a) Orthogonal quality and (b) Skewness Orthogonal quality has a maximum value of 1 and minimum value of 0, Skewness has to be close to zero. Skewness equaling 1 is deemed as inferior quality mesh.

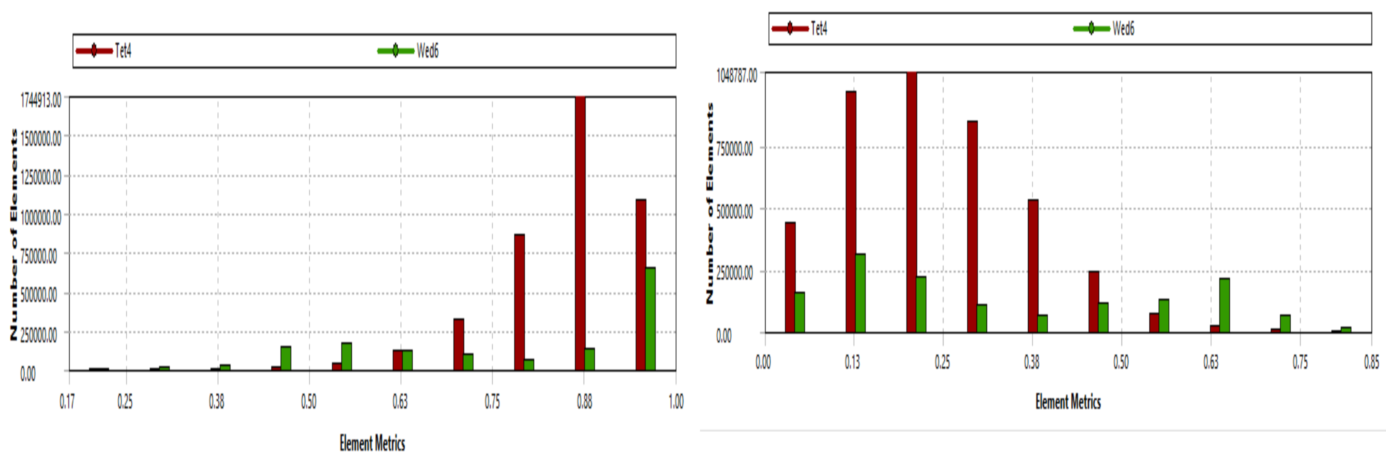

Figure 5.3 mesh metrics orthogonal quality (left) skewness (right)

Here we can see from graph figure 5.3 the most of element have in the range of [0.15-1] and skewness [0.95 - 0] which is in the acceptable range

5.3 Physical Setup with Ansys Pre-Processing

In this section the essentials of the ANSYS Pre setup are presented. The flow field is expressed by the continuity and incompressible Reynolds-averaged Navier–Stokes equations, the Transition SST turbulence model is used in the analysis of turbulent flow [37]. In the analysis of turbulent flow the y+ values are in the range of 0.0127 to 0.4567 which is the acceptable range for SST Turbulence model ($y+ < 1$) [25]. First-order numerical scheme is used to compute the convection and diffusion terms [38]. Velocity inlet and pressure outlet boundaries have been defined at the upstream face and downstream face of the outer cylinder respectively. Symmetry boundary condition has been assigned to the curved surface of the outer cylinder. The rotor faces have been assigned wall/no-slip boundary condition. The mean velocity at the inlet has been given as 6 m/s (rated wind Speed). Turbulence intensity of 5% has been chosen. In the pressure outlet, gauge pressure has been set to zero and the same turbulence intensity (5%). [37] The faces of the inner cylinder serve as an interface between Stationary and rotating part of the model. The standard pressure correction method and a first order upwind scheme was used. All walls were set to be no-slip boundaries. The rotor blades and the hub were set as moving wall attached to moving frame.

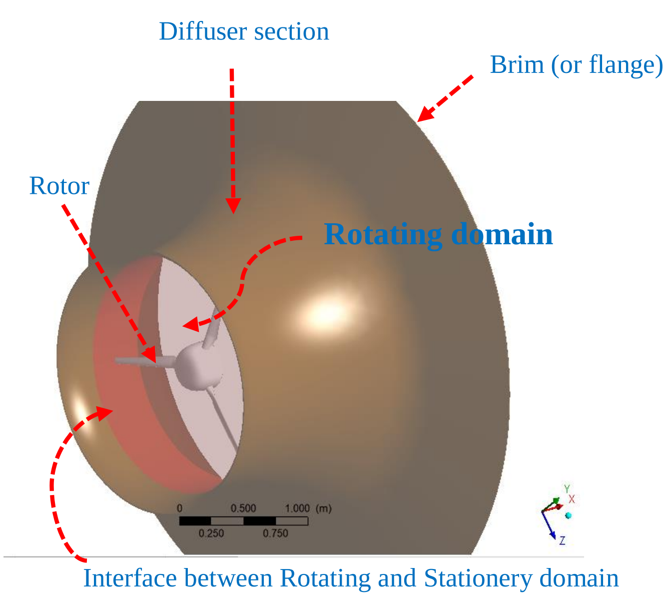

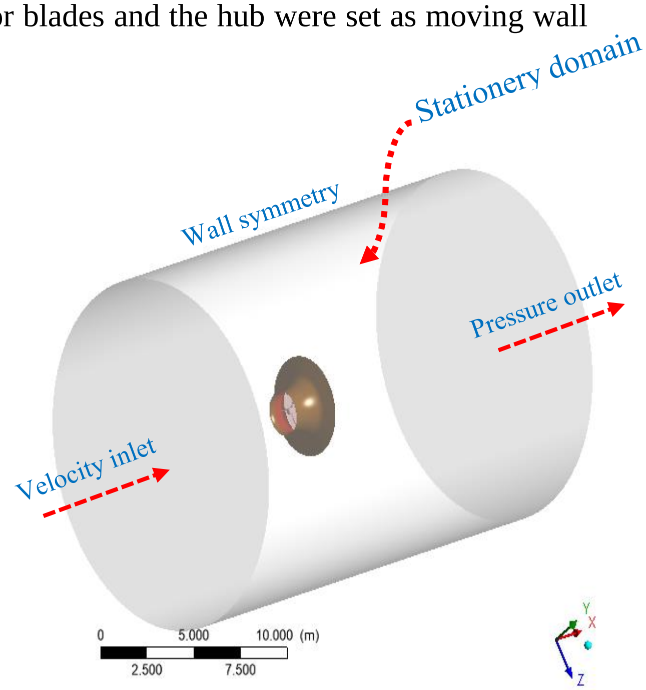

Figure 5.4 Boundaries Applied on the domains (right) and closed up view Brim Diffuser with rotor (left)

The rotating zone has been selected as the inner cylinder and the moving reference frame option has been enabled. Corresponding to the tip speed ratio of six, which is 63.33 rad / sec this angular velocity has been given for the inner domain fluid similar method can be found in [39].Time steps are used for an unsteady flow where the properties of the flow varies with time, that mean specification of time between each iterative solve. Total flow time for turbomachinery [in this case wind turbine] is the ratio of to rotational speed of rotor [40]. The time step used for the analysis was 1/20 total time, which corresponds to 0.005sec to capture 20-time points per rotation. The interface type between the stationary and rotating domains was Fluid-Fluid and Defining expressions is a good way of streamlining a CFD case [41] The following expressions in Table 5.1 are used in the setup. This way of defining expressions can be also found in the literatures

Table 5.1 Expression defined in ANSYS Fluent

Name	Expressions	Description
Rotor radius (r)	$0.9m$	Turbine radius
Tip speed ratio (λ)	6	The ratio of tip velocity to free stream velocity
Free steam velocity (V_0)	$6m/s$	Velocity of the wind
Omega (ω)	$\left(\frac{\lambda V_0}{r}\right)[rad/\sec]$	Angular velocity rotation in negative direction
Torque at rotor	**Torque_x@rotor**	The entire rotor is selected
Total time	$\left(2pi/omega\right)[\sec]$	Total simulation time

5.4 CFD Result and discussion

The following are results gathered from conducting a CFD analysis. the main objective of the present work is to determine the maximum torque that is generated from wind turbine

5.1.4.1Convergence of Torque

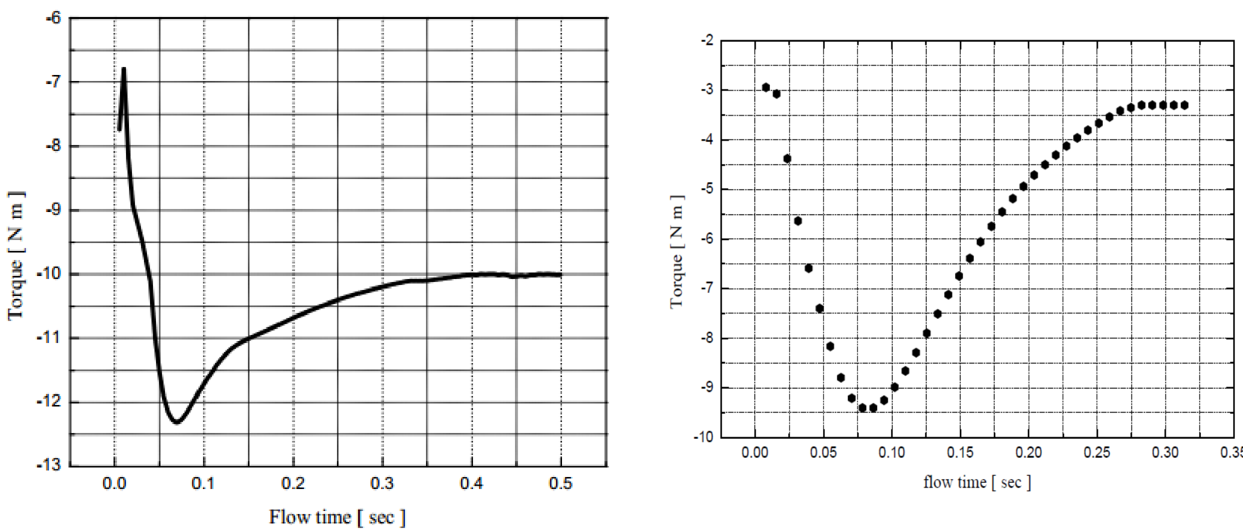

Fig.5.5 Torque vs flow time for the time step size of 0.005 sec for DAWTs (left) and bare wind turbine (right) for the time step size of 0.00785 sec

The shape of the torque curve is also similar to the earlier studies by different authors [42]. The early stage of the simulation obtained by using the time step of 0.005 sec for DAWT and the time step for bare wind turbine is 0.00875 sec is shown in Figure 5.5. The torque generated by the wind turbine as function of time tend to steady state value at $-10Nm$ for DAWTs and $-3Nm$ for bare wind turbine with a very small fluctuation for the same swept area and approaching wind speed due to the pressure drop and viscous effects. The power extracted by the diffuser augmented wind turbine can be determined using the calculated torque (T) and the rotor speed (Ω) which is $P_{ext} = T\Omega = 633W$ and for bare wind turbine $P_{ext} = T\Omega = 132.0908W$. Therefore, the optimized shrouded wind turbine increases the velocity and power augmentation by a factor of 1.58 and 3.78 respectively when compared to the performance of an unshrouded wind turbine with the same swept area and wind speed.

The available power for diffuser augmented wind turbine

$P_{av} = \frac{1}{2}\left(\rho A(\gamma V_0)^3\right) = 1557.83W$ Where $V_0 = 6m/s$, $\gamma = 1.67$, $D_r = 1.8m$ and $\rho = 1.204kg/m^3$ the available power for bare wind turbine is $P_{av} = \frac{1}{2}\left(\rho A(V_0)^3\right) = 336.491W$ the only different is velocity speed up ratio $(\gamma = 1)$. The power coefficient of for diffuser augmented wind turbine (DAWT) is the ratio of the extracted power to the available power which is $C_p = P_{ext}/P_{av} = 0.4065$ but for bare wind turbine the power coefficient of for bare wind turbine $C_p = 0.3925$ with the same rotor area and approaching wins speed the main reason for the difference is the reduction of tip loss in diffuser augmented wind turbine due to the presence of diffuser

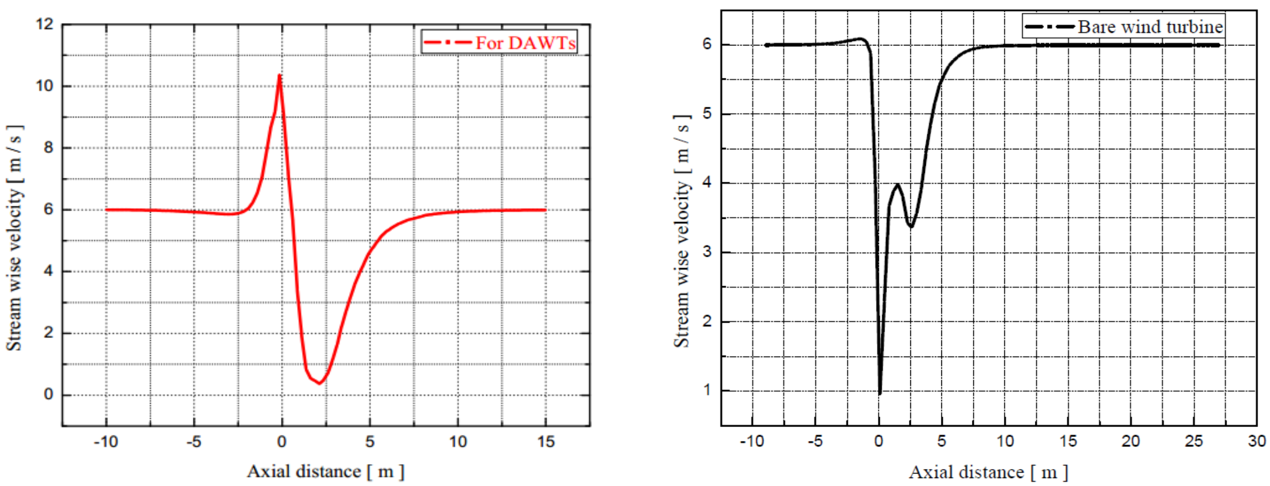

Figure 5.6 Streamwise Velocity distribution along a computational domain at y = 0.2 m and z = 0 m

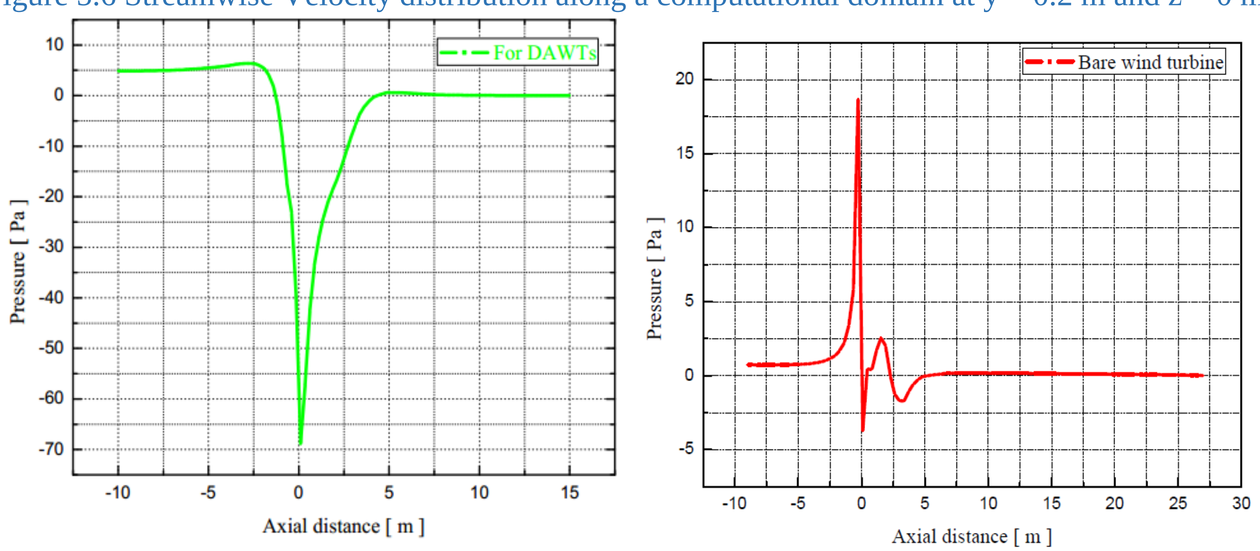

Figure 5.7 Pressure distribution along a computational domain at y = 0.2 m and z = 0 m

Figure 5.6 to 5.7 shows that the average velocity at the rotor plane would increase from $6ms^{-1}$ to $10ms^{-1}$ which represent 66.67% velocity augmentation is achieved. And its shows velocity and pressure distributions for DAWT and bare wind turbine at air passing the turbine rotor, brim diffuser and its domain at $\lambda = 6$. The relative static pressure at the diffuser outlet. The pressure behind the bare turbine is recovered quickly to the atmospheric value but at the outlet of the diffuser is still much lower than atmospheric pressure. It should be noted that the pressure is not uniform. The pressure variation and velocity distribution happened with the flow as a result of blade obstructing the flow which is shown the following figures

5.1.4.3 Pressure and velocity contour across the blade and brim diffuser

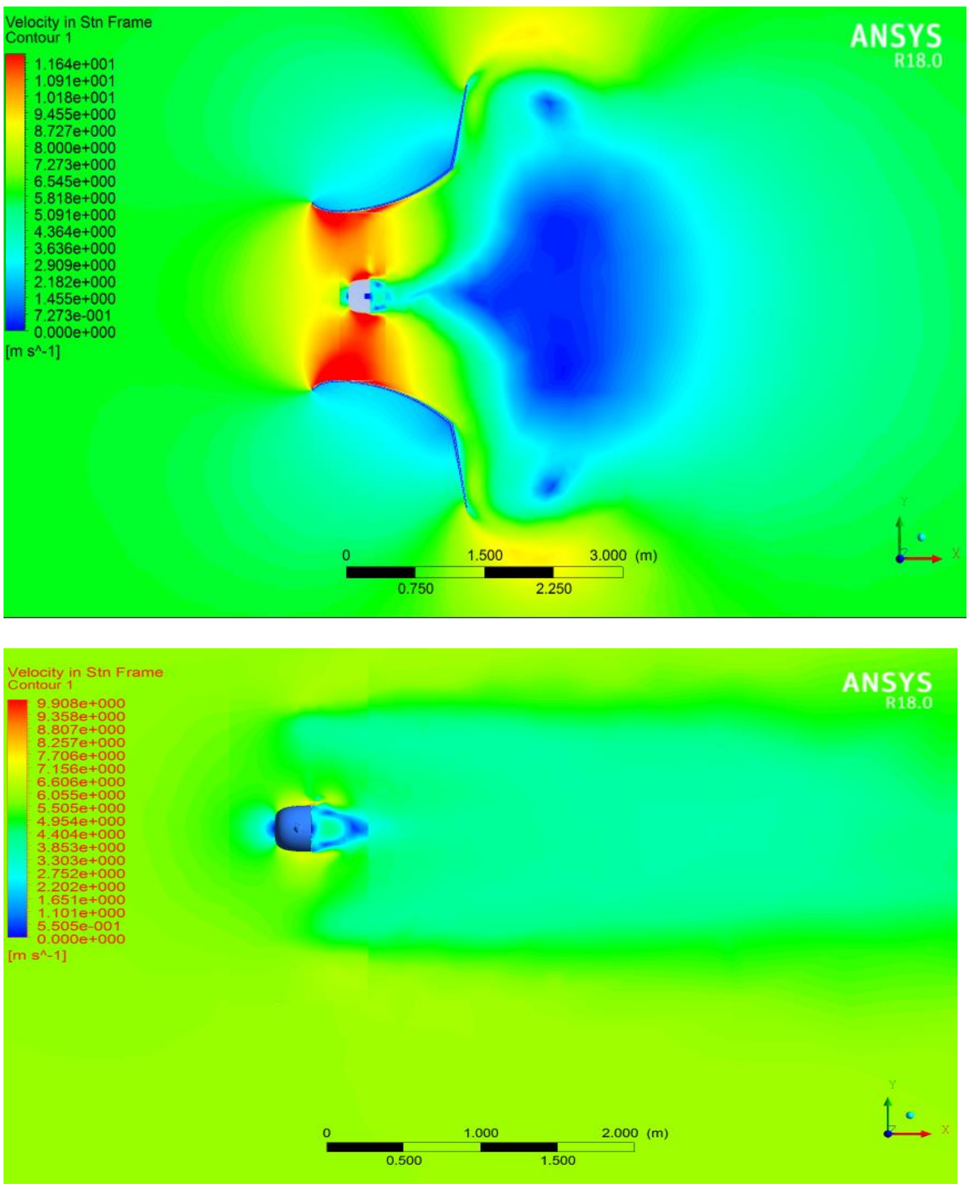

Figure 5.8 velocity distribution in DAWT (upper) and BWT (lower).

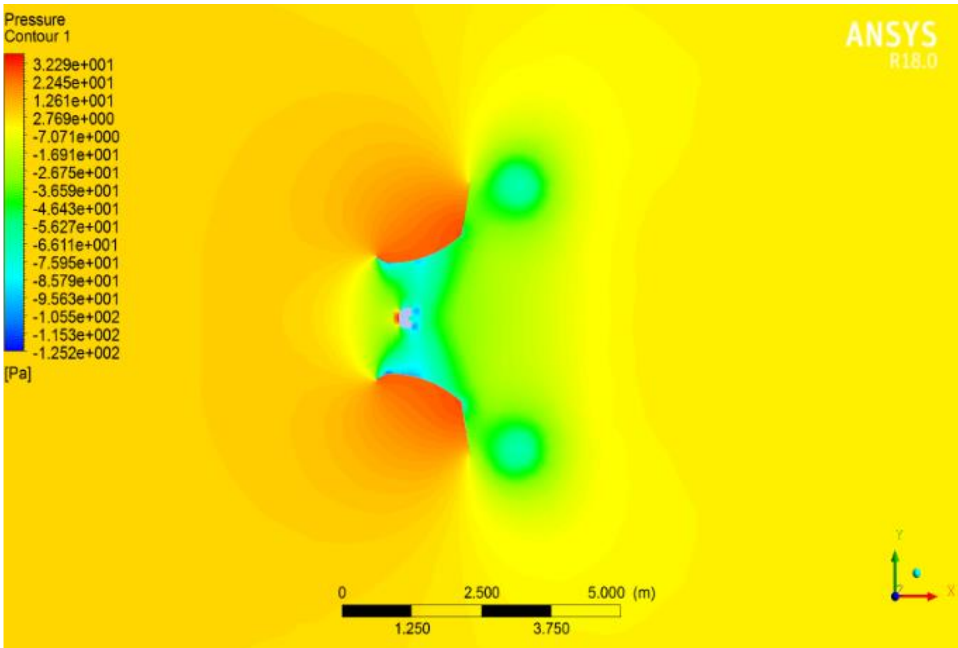

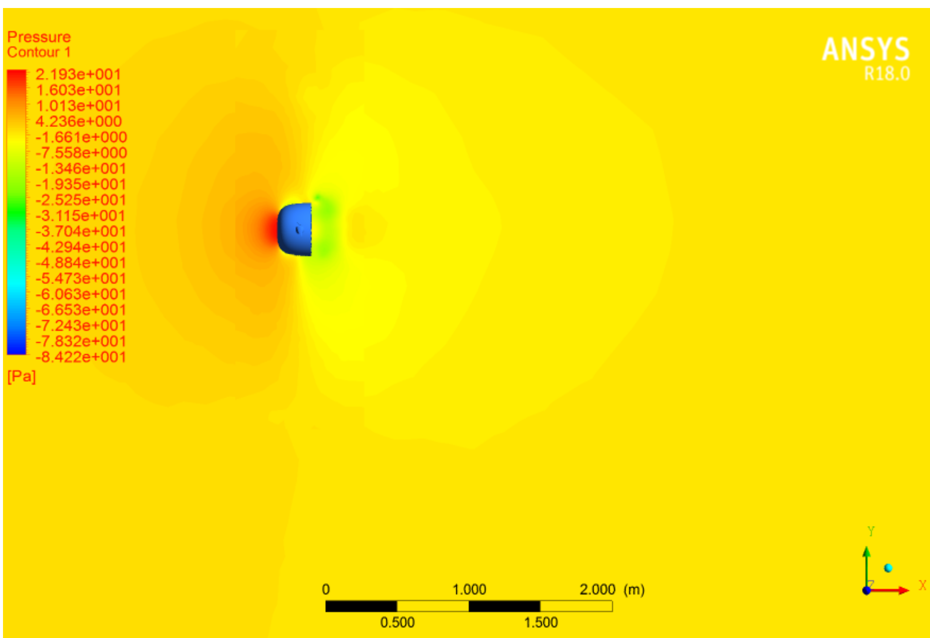

Figure 5.9 Pressure distributions in DAWT (upper) and BWT (lower).

From the above Figures and graphs, it's clear show that the pressure distribution in DAWTs at the front face seems evidently to be higher than the pressure distribution of bare wind turbine This significant drop in pressure cause the blade to spin clockwise.

5.1.4.4 Velocity vector across the blade

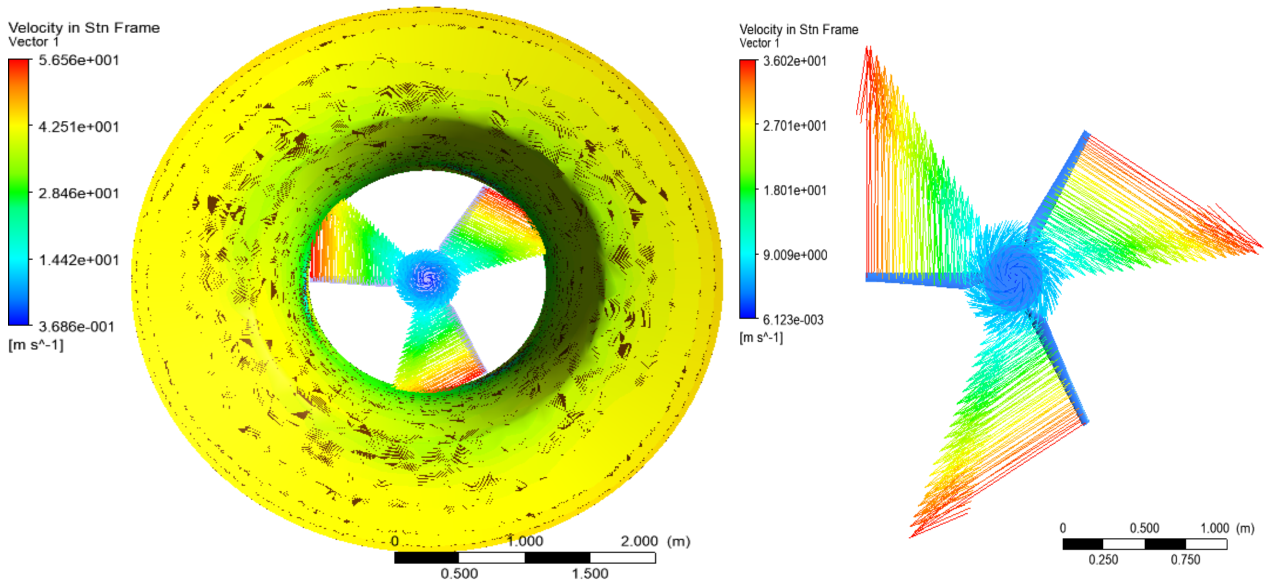

Figure 5.10 Velocity vectors across the blade for DAWTs (left) and bare wind turbine (right)

Figure 5.10 shows that the velocity vectors across the blade Velocity at the tip of the blade is more than the regions adjacent to the root and blade velocity at the tip for diffuser augmented wind turbine (DAWTs) is higher than bare wind turbine (BWTs) due to velocity augmentations of brim diffuser.

5.5 Validation of Numerical Analysis with Analytical

The FSI (Fluid Structure Interaction) on the Wind Turbine problem has been successfully completed and the results are verified with the analytical hand calculations.

Following are the conclusive findings:

- The blade velocity from the hand calculation is found to be 57m/s and from the CFD analysis it is 56.56m/s (indicated in Figure 5.10)
- The error is found to be 0.77% which can be ignored without seriously affecting the solution accuracy. Therefore, the CFD calculation has been analytically verified.

CHAPTER SIX

6 MANUFACTURING OF THE PROTOTYPE AND EXPERMENTAL TESTING

This chapter describes the 3D Print or manufacturing and testing procedure for the diffuser augmented wind turbine model. Each component and its assembling drawing of DAWT using a 3D CAD tool solid work 2016 and CAD visuals of each components and its assembling viewed in Appendix D–Drawing. The brim diffuser manufacturing activities were carried out at local workshop and the rotor was printed with 3D printer machine found in Minister of Science and Technology and dynamo which were purchased from the local market.

6.1 Wind turbine Blade and hub manufacturing process

3D CAD model of the optimized three blades turbine and hub geometry was printed with 3D Printer machine found in Minister of Science and Technology. With a material of Acrylonitrile Butadiene Styrene (ABS) plastic. Figure 6.1 shows photograph of 3D printed model of the optimized geometry of the blades with its hub.

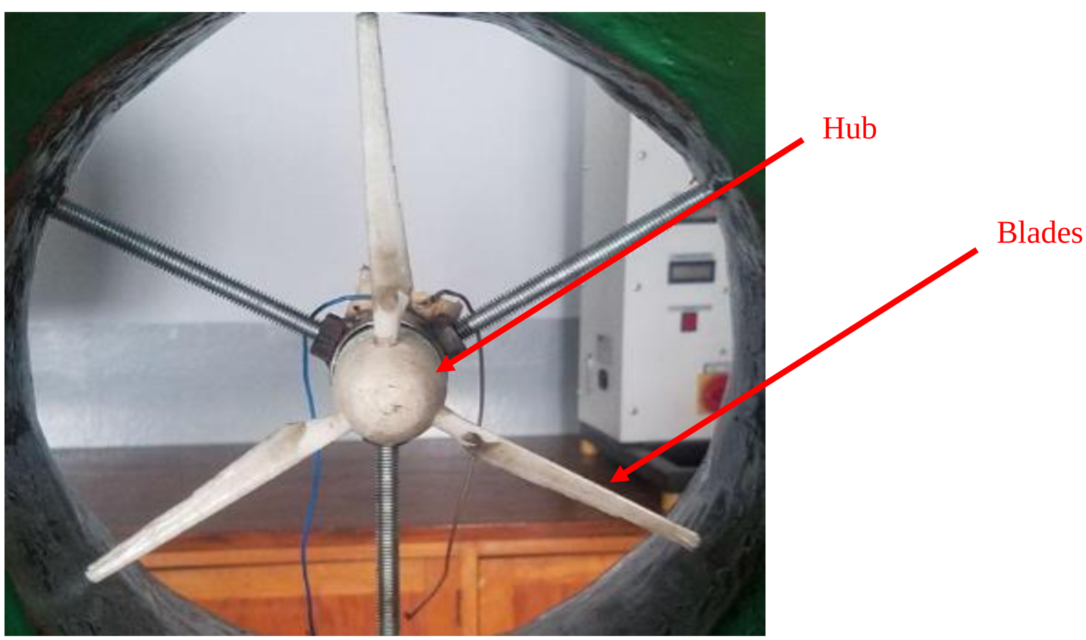

Figure 6.1: Views of 3D printed model of blades with hub

Material: *blade and hub geometry were printed with 3D Printer machine with a material of ABS and the* diffuser part were fabricated from commercial sheet metal which is very available in the local market.

6.2 Brim diffuser manufacturing process

First prepare a layout of the complete surface of a three-dimensional object of a brim diffuser on a plane which means formulate the development of the surface or flat pattern of the object. The development of surfaces is very important in the fabrication of brim diffuser. In making the development of a surface, an opening of the surface should be determined first. Every line used in making the development must represent the true length of the line (edge) on the object.

The steps to be followed for making a brim diffuser, using sheet metal are given below:

1. Draw the orthographic views of the object to full size.
2. Draw the development on a sheet of paper.
3. Transfer the development to the sheet metal.
4. Cut the development from the sheet.
5. Form the shape of the brim diffuser by bending.
6. Join the closing edges.

After transfer the development to the sheet metal cut the sheet metal by hydraulic sheet metal cutter based the development on a sheet of paper and then roll and bend sheet metals into round and conical shape to gain the specific section shape of brim diffuser like inlet shroud, diffuser section and the rounded flange ring by using rolling machine. Next to join different section of brim diffuser by arc welding using high heat to melt the parts together and allowing them to cool causing fusion. And then by using grinding machine to get a precisely finish and shape of the given material with high surface quality and low surface roughness by using STAR MAX Fiber Putty shown in Figure 6.3 is a two-component polyester putty, especially used to fill pinholes, sand scratches, or small hollows on each section of brim diffuser especially on diffuser section because of its shape and lastly to remove a layer of material from the object that is developed in welding to make them smother by using sand paper.

Figure 6.3 Photographs of MIDO coating for filling of small holes

Figure 6.2 Different views of the model of brim diffuser with stand

Handler for rotor

Which used to make or positioned the rotor (contain blades and hub) and dynamo at the center of brim diffuser by using three screw with a dimeter of 10 mm

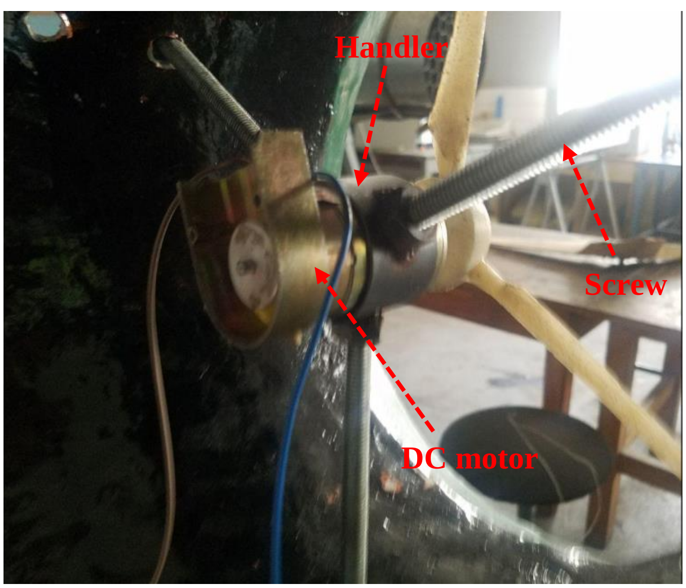

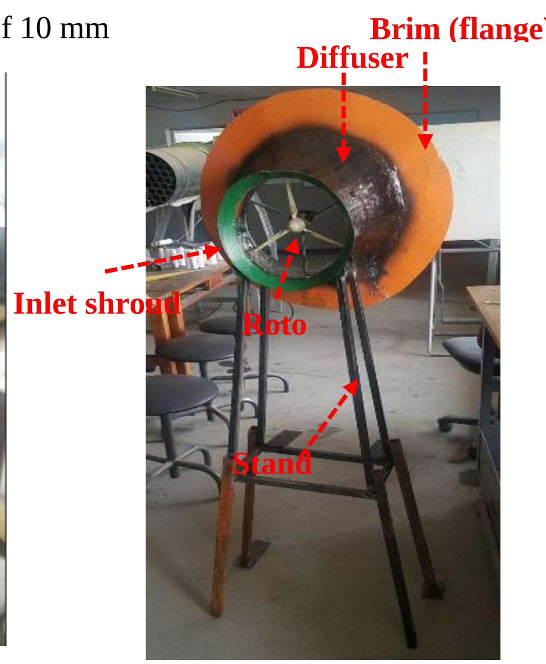

Figure 6.4 Photograph views of dynamo and rotor handler

Figure 6.5 Assemble drawing of diffuser augmented wind turbine (DWATs)

6.3 Measuring device

6.3.1 Environmental meter

This Environmental Meter Measures Humidity, Temperature, Air Velocity, Light and Sound level. Features contain: a dual LCD for simultaneously displaying Temperature and Air Velocity or Relative Humidity; Data Hold and Min/Max functions; a built-in low friction vane wheel which improves accuracy of air velocity, precision thin-film capacitance humidity sensor for fast response, and thermistor for ambient temperature. In this case which used to measure the wind speed of a fan.

Figure 6.6 Environmental meter

6.3.2 CLAMPMETER AND MULTIMETER

Which is also known as a volt-ohm-milliammeter is an electronic measuring instrument that combines several measurement functions in one unit. A typical multimeter can measure voltage, current, and resistance. Which measure dc voltage and current that developed from dc motor.

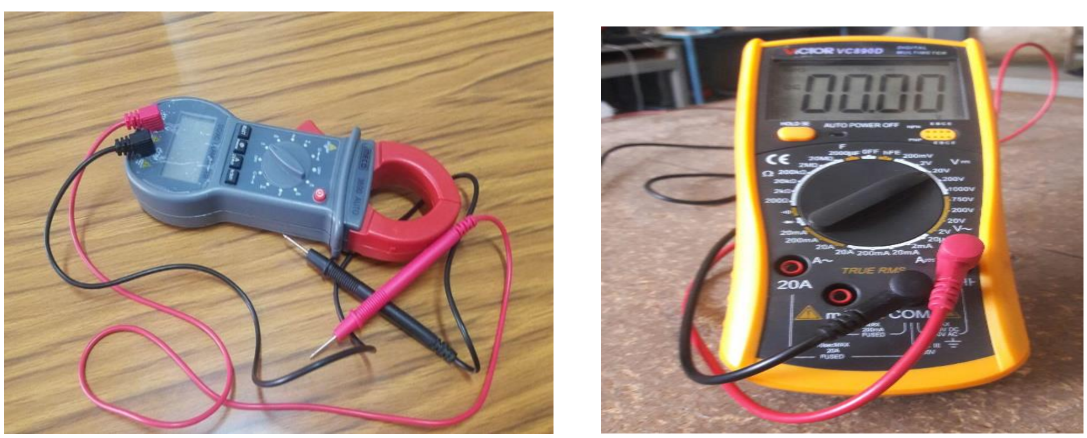

Figure 6.7 Photograph views of clamp meter (left) and multimeter (right)

6.3.3 Generator (dynamo)

A dynamo is an electrical generator. It works on the principle of using rotating coils to convert mechanical rotations into direct electric current. So, it used to convert rotation of turbine (mechanical energy) to electrical output, based on ohms' law where current equals voltage divided by resistance.

Figure 6.8 Photograph views of dynamo

6.4 Test Data Measurement Procedures

6.4.1 Measuring voltage

The steps to be followed to measuring voltage that developed from dynamo are given below:

1. Place your turbine in front of a fan and let it spin. It is normal for the voltage readings to fluctuate because of the inconsistent nature of the wind or unbalanced blades
2. Place a load in parallel with the multimeter so the dynamo is forced to do some work polarity is not relevant at this point
3. check the voltage, select DC volt (V) and set the number to 20
4. Voltage is related to how fast the dynamo is spinning. The faster it spins, the higher the voltage. With no load on dynamo, it has little resistance and can spin very fast.
5. We can measure voltage with no load and loading conditions

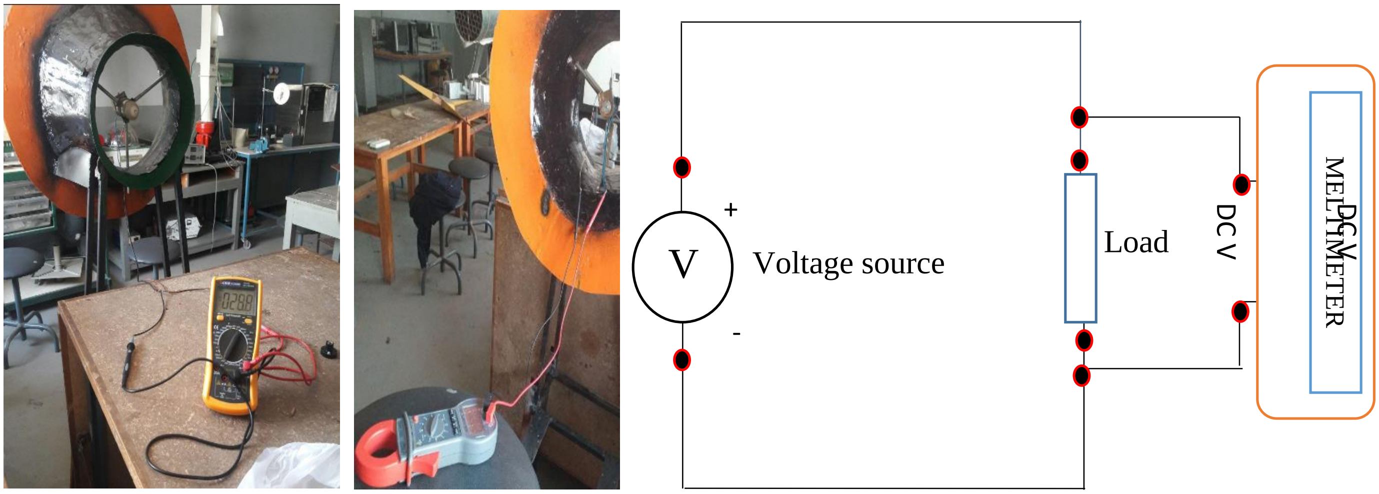

Figure 6.9 Clamp meter and multimeter connected in parallel with load to measure dc voltage setup (left) and its electrical circuit (right)

6.4.2 Measuring current

To calculate our turbine's power output, we will need to measure current as well. To measure current, place a load in series so the dynamo is forced to do some work. The current that our turbine produces depends on the load placed in the circuit and the torque our blades are generating.

The most common way to measure current in a circuit is to break the circuit open and insert a Load in series (in-line) with the circuit as shown in Figure 6.9. So that all electrons flowing through the circuit also have to go through the meter. Steps to Follow Using a Multi meter to Measure Current.

- Place a load in series with the millimeter so the dynamo is forced to do some work
- Set the meter to 200 or 20 mA, which is a typical range for our devices.
- The current that turbine produces depends on the load placed in the circuit and the torque generated by blades.
- measure Current with no load and loading conditions

Steps to Follow Using a Clamp meter to Measure Current

- Switch ON the meter and remove the probes (if attached)
- Select the DC current function using the dial

- Open the jaw-like structure using the side lever and insert the conductor through which the current is to be measured.

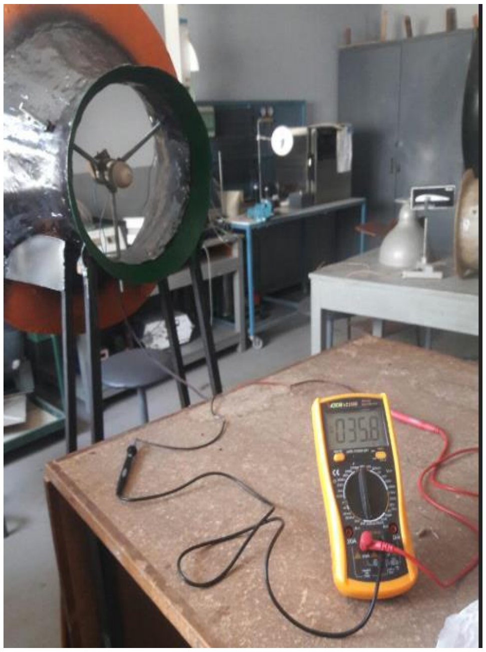

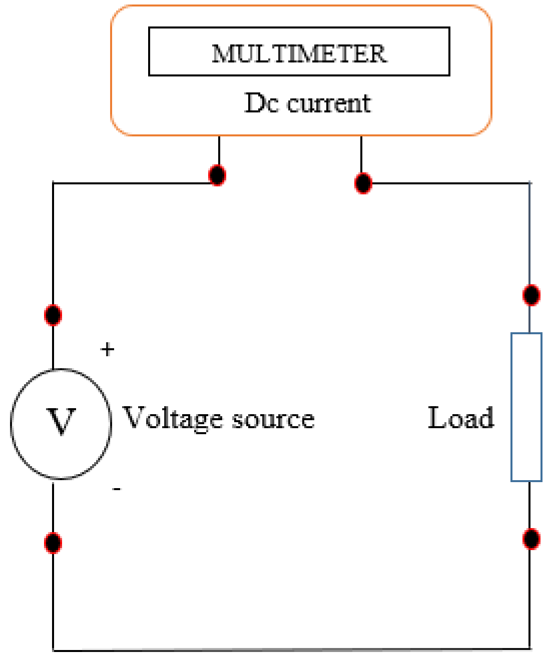

Figure 6.10 Multimeter connected in series with load to measure current flowing through it and its electrical circuit

6.5 Experimental Result and discussion

The result from measuring of output dc voltage from reading of multimeter is show below

Table 6.1 Experimental data obtained from diffuser augmented wind turbine at No –load and loading condition

measured Wind speed [m / s]	Loading condition	Measured Dc current [A]	measured Dc voltage [V]	Calculated Electrical power $E_p = VI$	Efficiency of dynamo η_d	Mechanical power $m_p = \frac{E_p}{\eta_d}$
5	No load	0.004	12.1	0.0484	0.8	0.0605
5	10ohm	0.784	4.98	3.90432	0.8	4.8804

6.5.1 Determining the power output of the model of diffuser augmented wind turbine

The terminal voltage when load current is drawn is called load voltage. The no load voltage is the terminal voltage when almost zero current is drawn from the supply. Table 6.1shows that under no load condition no load voltage is 12.1 volt and current will be nearly zero amperage that mean no current is draw in the circuit and under loading condition the voltage developed by turbine is 4.98 volt and the generated current in the circuit is 0.784A. Hence the electrical power output of turbine is a multiplication of voltage and current which is 3.90432 watt and dc motor efficiency is the ratio between the power available at the dc motor output and the energy supplied at the dc motor input. the efficiency of dc motor is $\eta_{dc} = 0.8$ [43]. Therefore, the mechanical power value is 4.8804watt.

6.6 Comparison of the CFD and the Experimental Results

Although the diffuser augmented wind turbine model is installed in laboratory and the electrical power of the turbine has been measured experimentally, a direct comparison between numerical and experimental results was not easy. The measured power available at output of a dc motor is the net electrical power after all losses such as core, copper and mechanical losses. The input to a generator is a mechanical input, this mechanical input is acquired by turbine blades, which are driven by wind speed. While the mechanical power of the turbine can be calculated numerically. A scaled down geometry of DAWT is used during the simulation. The mechanical power was calculated numerically in ANSYS Fluent. A detailed explanation and the procedure of the prototype 3D analysis based on CFD is included in Chapter 5, therefore it is not repeated here, but the converges of torque and its velocity augmentations is show below.

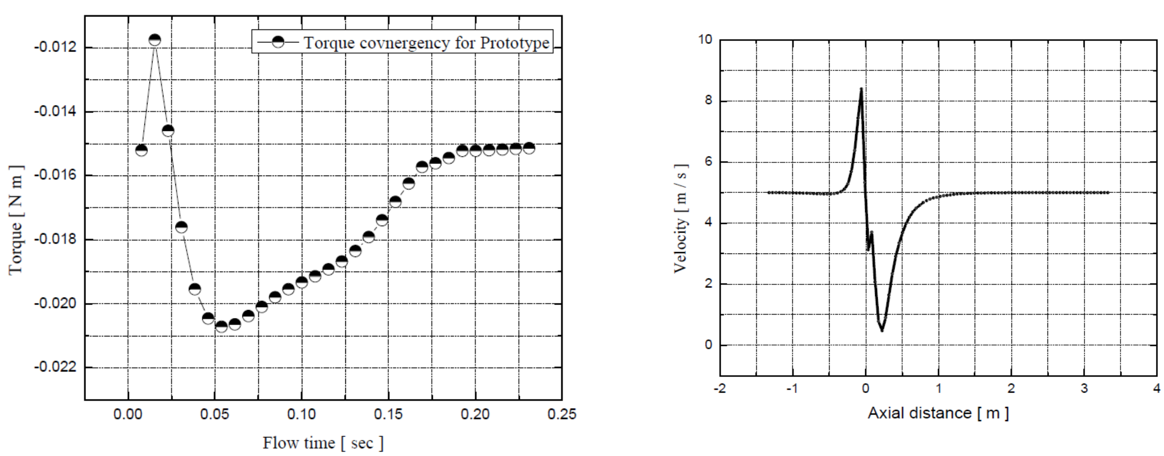

Figure 6.11 Torque vs flow time for the time step size of 0.055 sec for DAWTs (left)

Figure 6.11 the torque generated by the wind turbine as function of time tend to steady state value of – 0.01529Nm for prototype DAWTs. Therefore, the mechanical power is the product of torque that developed from turbine times its Angular rotation which is 408 rad / s. its value is 6.23832 Nm. The numerical and experimental result is shown in Table 6.2.

Table 6.2 The operating conditions, numerical and experimental data value

Wind speed [v] $[m/s]$	**radius [r]** $[cm]$	**CFD DSR** (γ)	**Available Power** P_{avl}	**CFD Mechanical Power** $P_{mech(CFD)}$	**Experimental Electrical P** $P_{elec(EXPT)}$	**Experimental Mechanical Power** $P_{mech(EXPT)}$	**Relative Error**
5	12.5	8.3	18.4549	**6.23832**	3.90432	**4.8804**	0.21

From Table 6.1 it shows that the result of CFD models over - predict with that of the experiments. An over-prediction is truly expected because the model does not account for various losses. These losses are mainly caused by the following reasons

- The quality of manufactured brim diffuser and 3D printed blades and hub
- In experimental set up the size of a domain (or the size of wind tunnel) much less than numerical set up.
- There can be also human and instrumental errors in experimental testing. These losses were not included in the CFD model.
- In CFD analysis encounter discretization, linearization, and round of error to solve a numerical solution of the differential equations in the use of computational methods.

This will lead to increase the variation of result between CFD with experimental model. However, based experimental results, it is evident that power output of the turbine is close enough to be validated. This shows that the optimized design is the best in terms of lowering the manufacturing cost of the diffuser augmented wind turbine.

CHAPTER SEVEN

6. CONCLUSIONS AND RECOMMENDATIONS

This chapter includes a summary of the critical relevant information of the research and recommendations for future work are also provided.

6.1 CONCLUSIONS

In this research, numerical analysis of shrouded wind turbine to investigate the flow field around the flanged diffuser and the variations of velocity up due to reconfiguration of brim diffuser at various flange angles and Subsequently, a MATLAB code was developed to obtain chord and twist angle distributions in the presence of a diffuser was established based on extended blade element momentum theory (EBEMT). Next, the Performance evaluation of diffuser augmented wind turbine (DAWT) was accomplished with the help of CFD analysis tools. The simulation is performed on the assembling of hub, blades and brim diffuser that is done by solid work and manufacture the model of DAWTs and model turbine was tested to verify the accuracy of CFD simulation. Based on the above numerical and experimental analysis and discussion the following conclusion is obtained.

1. About more 7 % velocity augmentation is achieved in the curved shape of diffuser than a straight diffuser. Therefore, the velocity augmentation and reduction of the size of a flanged diffuser is very important in the development of small-scale horizontal axis wind turbine shrouded by a brim diffuser.
2. From different flange angles for the curved sectional shape of brim diffuser, the optimum flange angle is obtained at 10^{o} angle, which gives higher velocity augmentation by 4 % when compared to normal flange angel due to the creation of low - pressure region behind the flange which increases mass flow rate through the diffuser. Therefore, the expected generated power by 10^{o} flange angel shrouded wind turbine for curved diffuser can reach 3 % more compared with normal $\left(0^{0}\right)$ flange angel.
3. The nature of the flow separation points inside of a diffuser greatly affect the acceleration of airflow through the brimmed diffuser
4. Power augmentation of the optimized brim diffuser shrouded wind turbine is a four - time increase than a conventional bare wind turbine (wind turbine without brim diffuser)

with velocity augmentation 66.6% achieved. With the same swept area and wind speed. Therefore, the power augmentation is very important in the development of small and middle scale horizontal axis wind turbine shrouded by a flanged diffuser.

5. The validation between experimental and numerical result of the prototype of a shrouded wind turbine is not enough good. This over prediction is because of varies loss that specified in section six.

6.2 RECOMMENDATIONS

According to the observation made during this research, the following recommendations can be reached that can be conducted for better prediction of the diffuser augmented wind turbine efficiency.

1. The manufacturing process of wind turbine blades was difficult as there is no experience in the country hence further manufacturing technology and methods should be studied for the casting of blades of a wind turbine.
2. The size of the model setup was small during the testing. It is suggested to increase the size of the wind tunnel.
3. Further manufacturing test and field test of the proposed shrouded wind turbine are needed to confirm the feasibility in practice.

REFERENCES

[1] A. Agha, H. N. Chaudhry, and F. Wang, "Diffuser Augmented Wind Turbine (DAWT) technologies: A review," *Int. J. Renew. Energy Res.*, vol. 8, no. 3, pp. 1369–1385, 2018.

[2] Z. H. Leghari and P. H. Shaikh, "Output Voltage Characteristics of Wind Energy System Considering Wind Speed and Number of Blades," no. January 2017, pp. 1–5, 2016.

[3] O. Ozgener and L. Ozgener, "Exergy and reliability analysis of wind turbine systems: A case study," *Renew. Sustain. Energy Rev.*, vol. 11, no. 8, pp. 1811–1826, 2007.

[4] H. Hirahara, M. Z. Hossain, M. Kawahashi, and Y. Nonomura, "Testing basic performance of a very small wind turbine designed for multi-purposes," *Renew. Energy*, vol. 30, no. 8, pp. 1279–1297, 2005.

[5] D. Y. C. Leung, Y. Deng, and M. K. H. Leung, "Design optimization of a cost-effective micro wind turbine," *WCE 2010 - World Congr. Eng. 2010*, vol. 2, no. Wce, pp. 988–993, 2010.

[6] K. Foreman, "Preliminary design and economic investigations of Diffuser Augmented Wind Turbines (DAWT)," *Final Report, 15 May 1979-31 Mar. 1980 …*, p. 28, 1981.

[7] T. Matsushima, S. Takagi, and S. Muroyama, "Characteristics of a highly efficient propeller type small wind turbine with a diffuser," *Renew. Energy*, vol. 31, no. 9, pp. 1343–1354, 2006.

[8] Y. Ohya, T. Karasudani, A. Sakurai, K. ichi Abe, and M. Inoue, "Development of a shrouded wind turbine with a flanged diffuser," *J. Wind Eng. Ind. Aerodyn.*, vol. 96, no. 5, pp. 524–539, 2008.

[9] S. A. H. Jafari and B. Kosasih, "Flow analysis of shrouded small wind turbine with a simple frustum diffuser with computational fluid dynamics simulations," *J. Wind Eng. Ind. Aerodyn.*, vol. 125, pp. 102–110, 2014.

[10] K. I. Abe and Y. Ohya, "An investigation of flow fields around flanged diffusers using CFD," *J. Wind Eng. Ind. Aerodyn.*, vol. 92, no. 3–4, pp. 315–330, 2004.

[11] S. A. H. Jafari and B. Kosasih, "Flow analysis of shrouded small wind turbine with a simple frustum diffuser with computational fluid dynamics simulations," *J. Wind Eng. Ind. Aerodyn.*, vol. 125, pp. 102–110, 2014.

[12] O. Igra, "Research and development for shrouded wind turbines," *Energy Convers. Manag.*, vol. 21, no. 1, pp. 13–48, 1981.

[13] B. Kosasih and H. Saleh Hudin, "Influence of inflow turbulence intensity on the performance of bare and diffuser-augmented micro wind turbine model," *Renew. Energy*, vol. 87, pp. 154–167, 2016.

[14] W. D. Lubitz and A. Shomer, "Wind Loads and Efficiency of a Diffuser Augmented Wind Turbine (DAWT)," *Proc. Can. Soc. Mech. Eng. Int. Congr. 2014*, pp. 1–5, 2014.

[15] Y. Liu and S. Yoshida, "An extension of the Generalized Actuator Disc Theory for aerodynamic analysis of the diffuser-augmented wind turbines," *Energy*, vol. 93, pp. 1852–1859, 2015.

[16] B. L. Gilbert and K. M. Foremant, "Experimental Demonstration of the Diff user-Augmented Wind Turbine Concept," vol. 3, no. 4, pp. 235–240, 1979.

[17] F. Bet and H. Grassmann, "Upgrading_Conventional_Wind_Turbines.Pdf," vol. 1, 2001.

[18] C.A.J.FLETCHER, "Diffuser Augmented Wind turbine Analysis." .

[19] A. Anzai, Y. Nemoto, and I. Ushiyama, "Wind tunnel analysis of concentrators for augmented wind turbines," *Wind Eng.*, vol. 28, no. 5, pp. 605–614, 2004.

[20] C. Harrington, "Real-time urban picture sought," *Jane's Def. Wkly.*, vol. 87, no. OCT., pp. 1116–1123, 2006.

[21] J. R. P. Vaz and D. H. Wood, "Aerodynamic optimization of the blades of diffuser-augmented wind turbines," *Energy Convers. Manag.*, vol. 123, pp. 35–45, 2016.

[22] J. F. Hu and W. X. Wang, "Upgrading a shrouded wind turbine with a self-adaptive flanged diffuser," *Energies*, vol. 8, no. 6, pp. 5319–5337, 2015.

[23] M. Shives and C. Crawford, "Computational Analysis of Ducted Turbine Performance,"

3rd Int. Conf. Ocean Energy, vol. 6, pp. 1–6, 2010.

[24] F. Owis, M .T. S. Badawy, K. A. Abed, H. E. Fawaz, and A. Elfeky, "Numerical Investigation of loaded and unloaded diffuser equipped with a flange," *Int. J. Sci. Eng. Res.*, vol. 6, no. 11, pp. 312–341, 2015.

[25] I. Shukla, S. S. Tupkari, A. K. Raman, and A. N. Mullick, "Wall Y+ approach for dealing with turbulent flow through a constant area duct," *AIP Conf. Proc.*, vol. 1440, no. May 2015, pp. 144–153, 2012.

[26] K. Abe *et al.*, "Experimental and numerical investigations of flow fields behind a small wind turbine with a flanged diffuser," *J. Wind Eng. Ind. Aerodyn.*, vol. 93, no. 12, pp. 951–970, 2005.

[27] L. André and B. Maia, "Experimental and Numerical study of a Diffuser Augmented Wind Turbine - DAWT Renewable Energies and Energy Efficiency Experimental and Numerical study of a Diffuser Augmented Wind Turbine - DAWT," no. December, p. 91, 2014.

[28] H. K. Jafari *et al.*, *ADVANCES IN WIND Edited by Rupp Carriveau*. 2012.

[29] J. R. P. Vaz and D. H. Wood, "Aerodynamic optimization of the blades of diffuser-augmented wind turbines," *Energy Convers. Manag.*, vol. 123, pp. 35–45, 2016.

[30] D. A. Tavares Dias Do Rio Vaz, A. L. Amarante Mesquita, J. R. Pinheiro Vaz, C. J. Cavalcante Blanco, and J. T. Pinho, "An extension of the Blade Element Momentum method applied to Diffuser Augmented Wind Turbines," *Energy Convers. Manag.*, vol. 87, pp. 1116–1123, 2014.

[31] Y. Liu and S. Yoshida, "An extension of the Generalized Actuator Disc Theory for aerodynamic analysis of the diffuser-augmented wind turbines," *Energy*, vol. 93, pp. 1852–1859, 2015.

[32] *Green Energy and Technology*. .

[33] S. Hjort and H. Larsen, "Rotor design for diffuser augmented wind turbines," *Energies*, vol. 8, no. 10, pp. 10736–10774, 2015.

[34] S. Jain, N. Sitaram, and S. Krishnaswamy, “Effect of reynolds number on aerodynamics of airfoil with gurney flap,” *Int. J. Rotating Mach.*, vol. 2015, no. 1, 2015.

[35] A. R. L. Francisco, “済無No Title No Title,” *J. Chem. Inf. Model.*, vol. 53, no. 9, pp. 1689–1699, 2013.

[36] A. Yadav and G. Lal, “CFD Analysis of S834 and S835 Airfoil for Application in Wind Turbine,” vol. 5, no. 03, pp. 834–836, 2017.

[37] S. A. H. Jafari and B. Kosasih, “Journal of Wind Engineering Flow analysis of shrouded small wind turbine with a simple frustum diffuser with computational fl uid dynamics simulations,” *Jnl. Wind Eng. Ind. Aerodyn.*, vol. 125, pp. 102–110, 2014.

[38] S. A. Jafari and B. Kosasih, “Analysis of the power augmentation mechanisms of diffuser shrouded micro wind turbine with computational fluid dynamics simulations,” *Wind Struct. An Int. J.*, vol. 19, no. 2, pp. 199–217, 2014.

[39] M. Keerthana, M. Sriramkrishnan, and A. Abraham, “AERODYNAMIC ANALYSIS OF A SMALL HORIZONTAL AXIS,” no. July, 2012.

[40] “Time Step Planning - Computational Fluid Dynamics is the Future.” .

[41] S. A. Jafari and B. Kosasih, “Analysis of the power augmentation mechanisms of diffuser shrouded micro wind turbine with computational fluid dynamics simulations,” *Wind Struct. An Int. J.*, vol. 19, no. 2, pp. 199–217, 2014.

[42] A. Namiranian, “3D Simulation of a 5MW Wind Turbine,” 2011.

[43] M. C. Options, “Table of Contents A : Motor Configuration Options B : Instrument Grade Brushless DC Servo Motors C : Automation Grade Brushless DC Servo Motors.”

LIST OF APPENDICES

Appendix A

Description of diffuser augmented wind turbine (DAWTs) and the CFD simulations. Design parameters used in the simulation of the DAWT

Parameter	values
Turbine diameter	1.8 m
Hub diameter	0.36 m
Number of blades	3
Blade airfoil	S835
Free stream velocity	6 m / s
Air density at 20^0c	1.225 kg / m^3
Rotational speed	604.8 rpm
Diffuser shape	cycloid
Speed up velocity ratio for brim diffuser (γ)	1.58
Power output	633 W

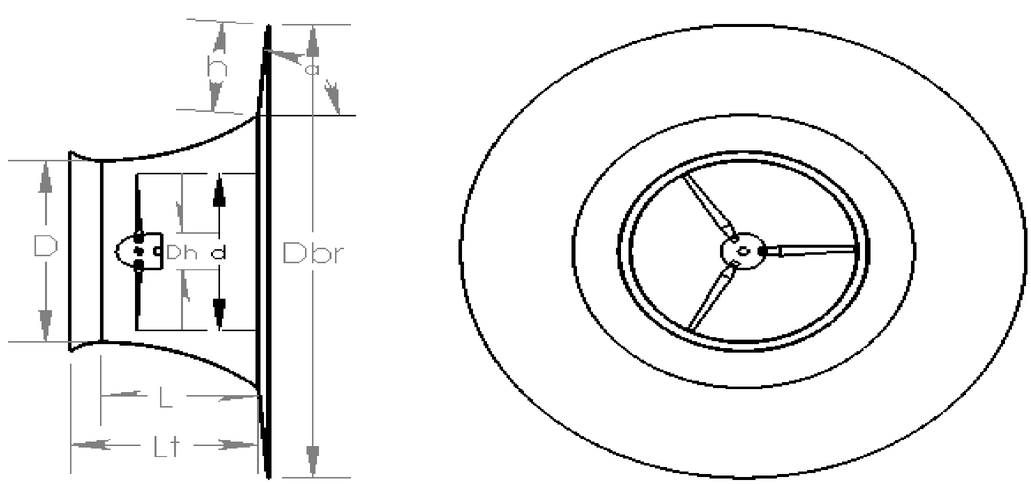

The virtual turbine shrouded with a brim diffuser

The dimension of brim diffuser

Parameter	values
Diameter Duct inlet, D	2m
Demeter of hub, Dh	0.36m
Rotor diameter, d	1.8 m
Diffuser length, L	1.26 m
Flange length, h	0.9 m
Brim diffuser length, Lt	1.15 m
Distance from inlet diffuser to rotor	0.55 m
Tip clearance	20mm

Appendix B

MATLAB code for rotor blade design for DAWTs

```
% this Program used to implement blade element/one-dimensional wake analysis for a diffuser
% augmented horizontal-axis wind turbine with any number of blades of any length which
gives
% the radius, chord, and twist distribution of the blade elements
% Function argument is
% Numb - number of blades
% Main variables are
% a - axial interference factor
% adash - rotational interference factor
% Cd - drag coefficient for S835
% Cl - lift coefficient for S835
% gamma - Speed-up ratio of diffuser
% delr - radial width of blade element
% VO - free stream Velocity (m/sec)
```

```
% aoa - angle of attack of blade element
% lambda - tip speed ratio (TSR)
% R- radius (meter)
% r_hub - radius of hub (Hub location) take 16% of rotor diameter
% chord - chord of blade element
% twist - angle of twist
clc
clear all
gamma = 1.7;
numb = 3;
Vo = 5;
lambda = 6;
R = 0.125;
r_hub = 0.036;
omega = Vo*lambda/R;
Cl = 0.91;
Cd = 0.0147;
aoa = 6.5*pi/180;
ai = 1/3;
adash= 0;
nbes = 15;
delr = (R-r_hub)/( nbes -1);
r_blade = r_hub:delr:R;
twist = 1:1:nbes;
Chord = 1:1:nbes;
figure('units','normalized','outerposition',[0 0 1 1])
for i=1: nbes
   a = ai;
   ap = adash;
   MAXerror = 0.00001;
   error = MAXerror + 0.001;
```

```
r = r_blade(1,i);
while error > MAXerror
   Phi = atan((gamma*Vo*(1-a))/(omega*r*(1+ap)));
   Cn = Cl*cos(Phi) + Cd*sin(Phi);
   Ct = Cl*sin(Phi) - Cd*cos(Phi);
   x = omega*r/Vo;
   B = 16;
   E = -24;
   S = 9-(3*(x/gamma)^2);
   H = ((x/gamma)^2)-1;
   I = roots([B E S H]);
   R = I(1,1);
   y = I(2,1);
   z = I(3,1);
   if R > 1
      R = 0;
   end
   if R < 0
      R = 0;
   end
   if y > 1
      y = 0;
   end
   if y < 0
      y = 0;
   end
   if z > 1
      z = 0;
   end
   if z < 0
      z = 0;
```

```
        end
        if R > 0
            a = R;
        end
        if y > 0
            a = y;
        end
        if z > 0
            a = z;
        end
        ap = (1 - (3*a))/((4*a) - 1);
        c = (8*pi*a*r*(sin(Phi))^2/( numb *Cn*(1-a)*gamma^2));
        twist_opt = (Phi - aoa)*180/pi;
        Phinew = atan((gamma*Vo*(1-a))/(omega*r*(1+ap)));
        Chord(1,i) = c;
        twist(1,i) = twist_opt;
        AxInd(1,i) = a;
        TangInd(1,i) = ai;
        error = abs(Phinew-Phi);
    end
end
subplot(1,2,1)
plot(r_blade,Chord,'r')
grid on
```

Appendix C

Coordinate of NREL's S835 Airfoil

1	0	0
0.995932	0.000974	0
0.984473	0.004552	0
0.967194	0.010971	0

0.945459	0.019503	0
0.919943	0.029016	0
0.890618	0.038526	0
0.857149	0.047861	0
0.819938	0.057178	0
0.779531	0.066312	0
0.736444	0.075033	0
0.691173	0.083101	0
0.644202	0.09028	0
0.596002	0.096359	0
0.547033	0.101147	0
0.497745	0.104476	0
0.448511	0.106196	0
0.399664	0.106378	0
0.351783	0.104999	0
0.305188	0.102105	0
0.260367	0.097834	0
0.217816	0.092265	0
0.177969	0.085485	0
0.141266	0.077587	0
0.108053	0.06868	0
0.078706	0.058894	0
0.053467	0.048379	0
0.032658	0.037351	0
0.016487	0.026032	0
0.005368	0.014774	0
0.003569	0.012203	0
0.001995	0.009465	0

0.000868	0.006772	0
0.000259	0.003974	0
0.00023	0.003763	0
0.000015	0.000995	0
0.001113	-0.008866	0
0.006381	-0.022529	0
0.015773	-0.036575	0
0.029084	-0.050332	0
0.046306	-0.063467	0
0.067214	-0.075502	0
0.091816	-0.086196	0
0.11982	-0.095194	0
0.151207	-0.102304	0
0.185631	-0.107229	0
0.223218	-0.109799	0
0.26372	-0.110144	0
0.306838	-0.108293	0
0.352267	-0.104298	0
0.399699	-0.098265	0
0.448814	-0.090357	0
0.499275	-0.08081	0
0.550725	-0.069931	0
0.602768	-0.05811	0
0.654962	-0.045821	0
0.706793	-0.033614	0
0.757643	-0.022112	0
0.806764	-0.011986	0
0.853241	-0.003934	0

0.895818	0.001265	0
0.932596	0.003434	0
0.962014	0.003325	0
0.983186	0.002036	0
0.995825	0.000638	0
1	0	0

Appendix D

Detail drawing of the components of diffuser augmented wind turbine

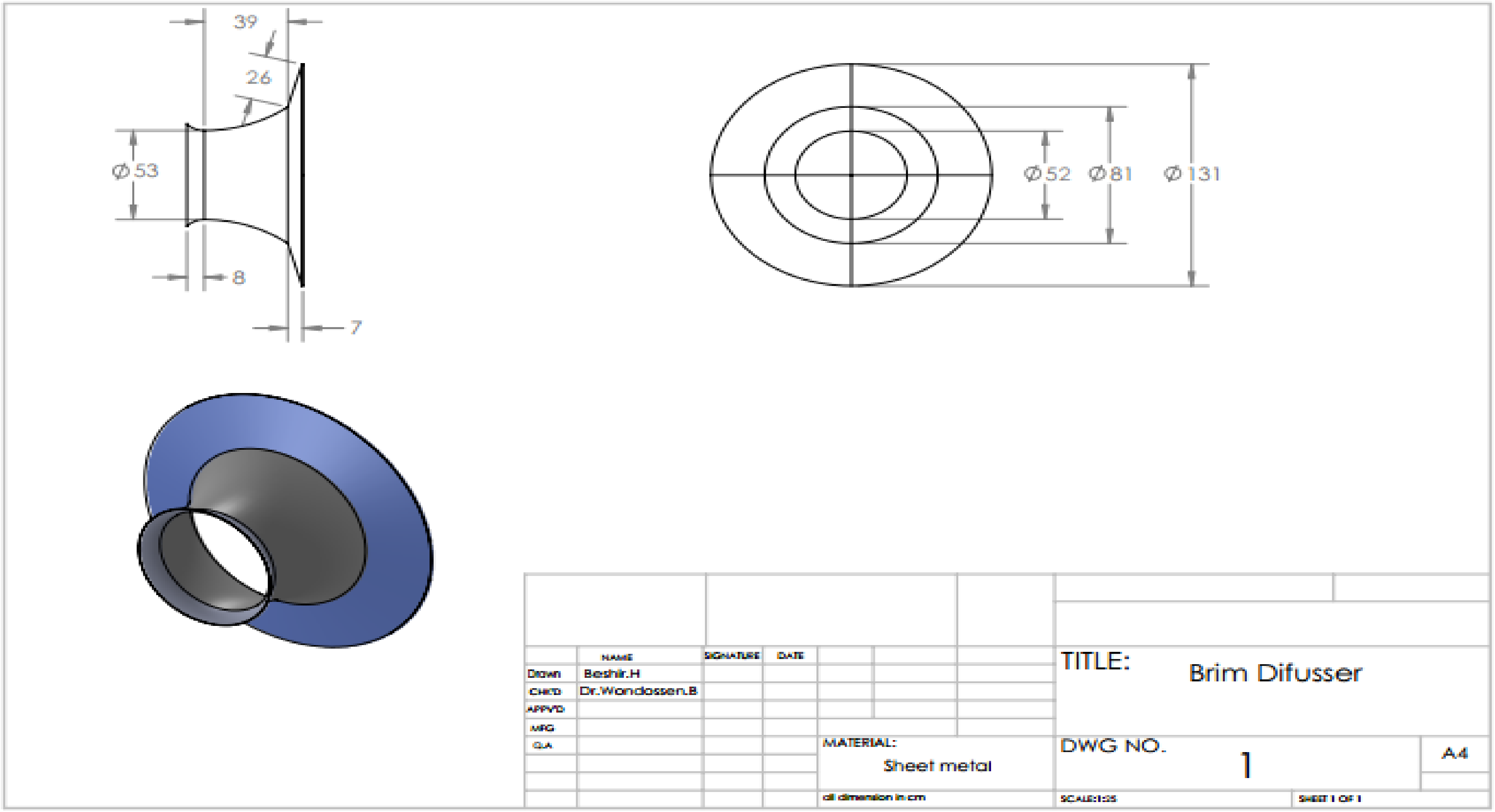

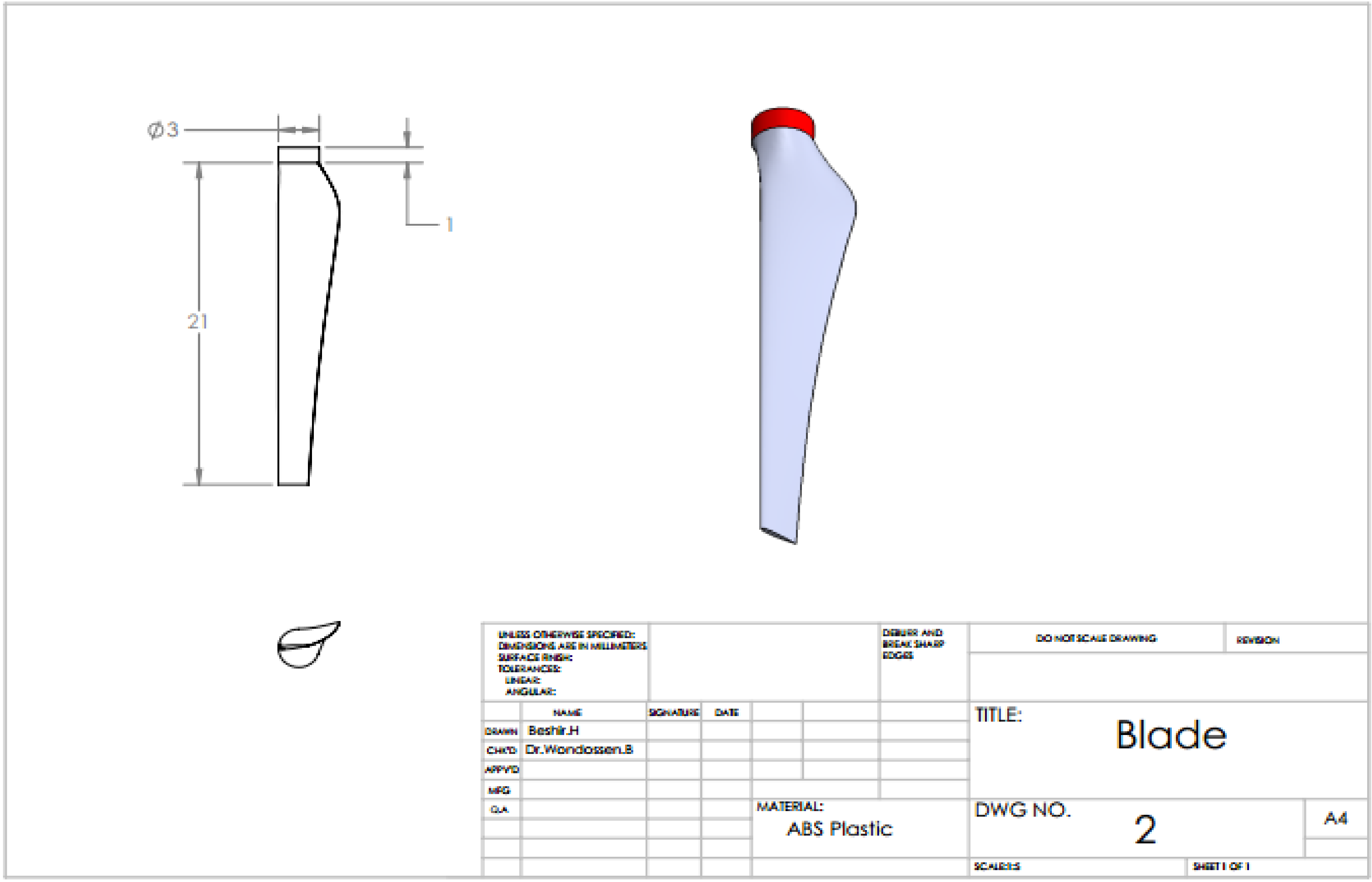
Ø3
1
21
UNLESS OTHERWISE SPECIFIED:
DIMENSIONS ARE IN MILLIMETERS
SURFACE FINISH:
TOLERANCES:
LINEAR:
ANGULAR:
DEBURR AND BREAK SHARP EDGES
DO NOT SCALE DRAWING
REVISION
NAME
SIGNATURE
DATE
DRAWN Beshir.H
CHK'D Dr.Wondossen.B
APPV'D
MFG
Q.A
TITLE:
Blade
MATERIAL:
ABS Plastic
DWG NO.
2
A4
SCALE:1:5
SHEET 1 OF 1

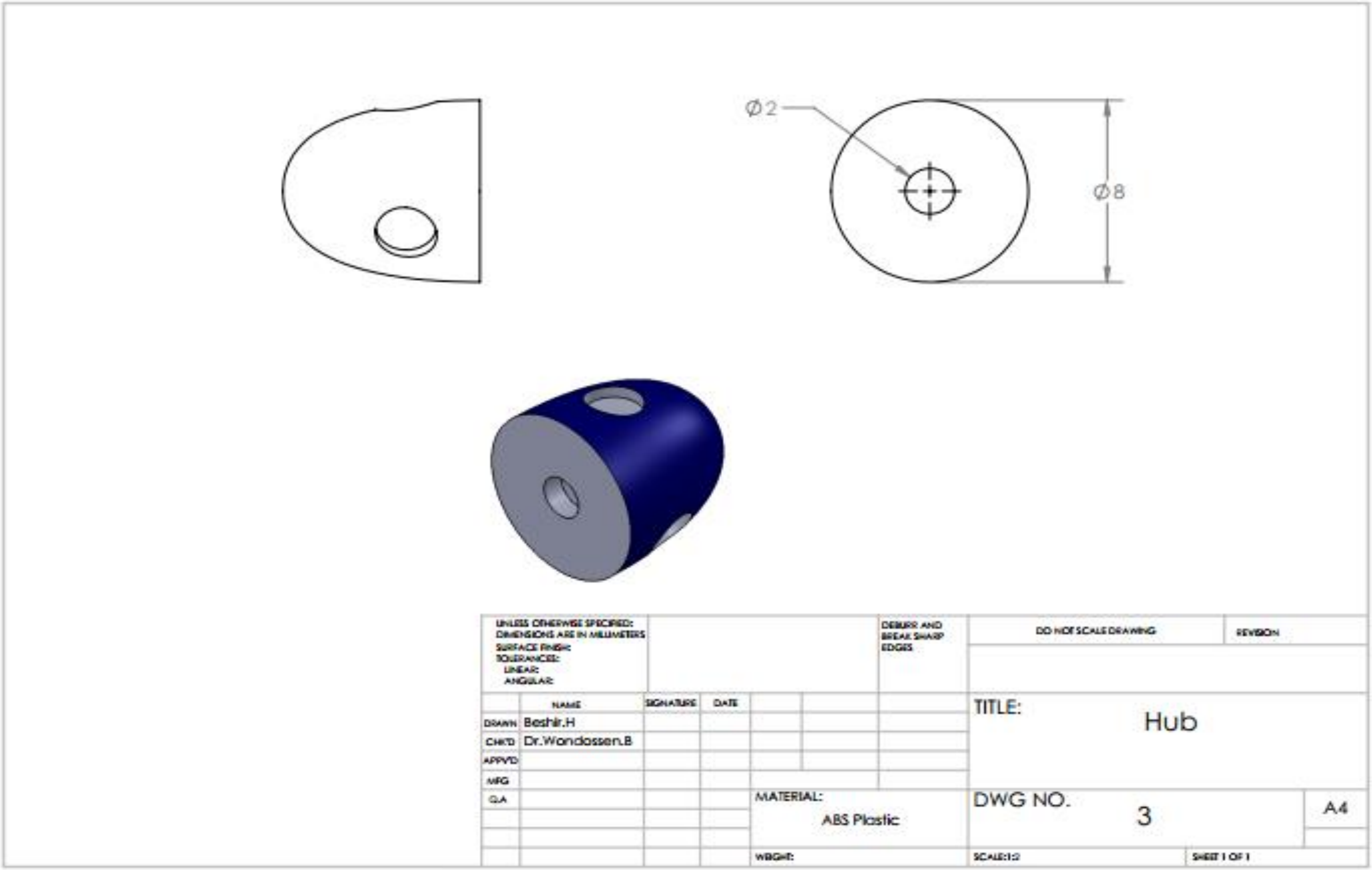
Ø2
Ø8
UNLESS OTHERWISE SPECIFIED:
DIMENSIONS ARE IN MILLIMETERS
SURFACE FINISH:
TOLERANCES:
LINEAR:
ANGULAR:
DEBURR AND BREAK SHARP EDGES
DO NOT SCALE DRAWING
REVISION
NAME
SIGNATURE
DATE
DRAWN Beshir.H
CHK'D Dr.Wondossen.B
APPV'D
MFG
Q.A
TITLE:
Hub
MATERIAL:
ABS Plastic
DWG NO.
3
A4
WEIGHT:
SCALE:1:2
SHEET 1 OF 1

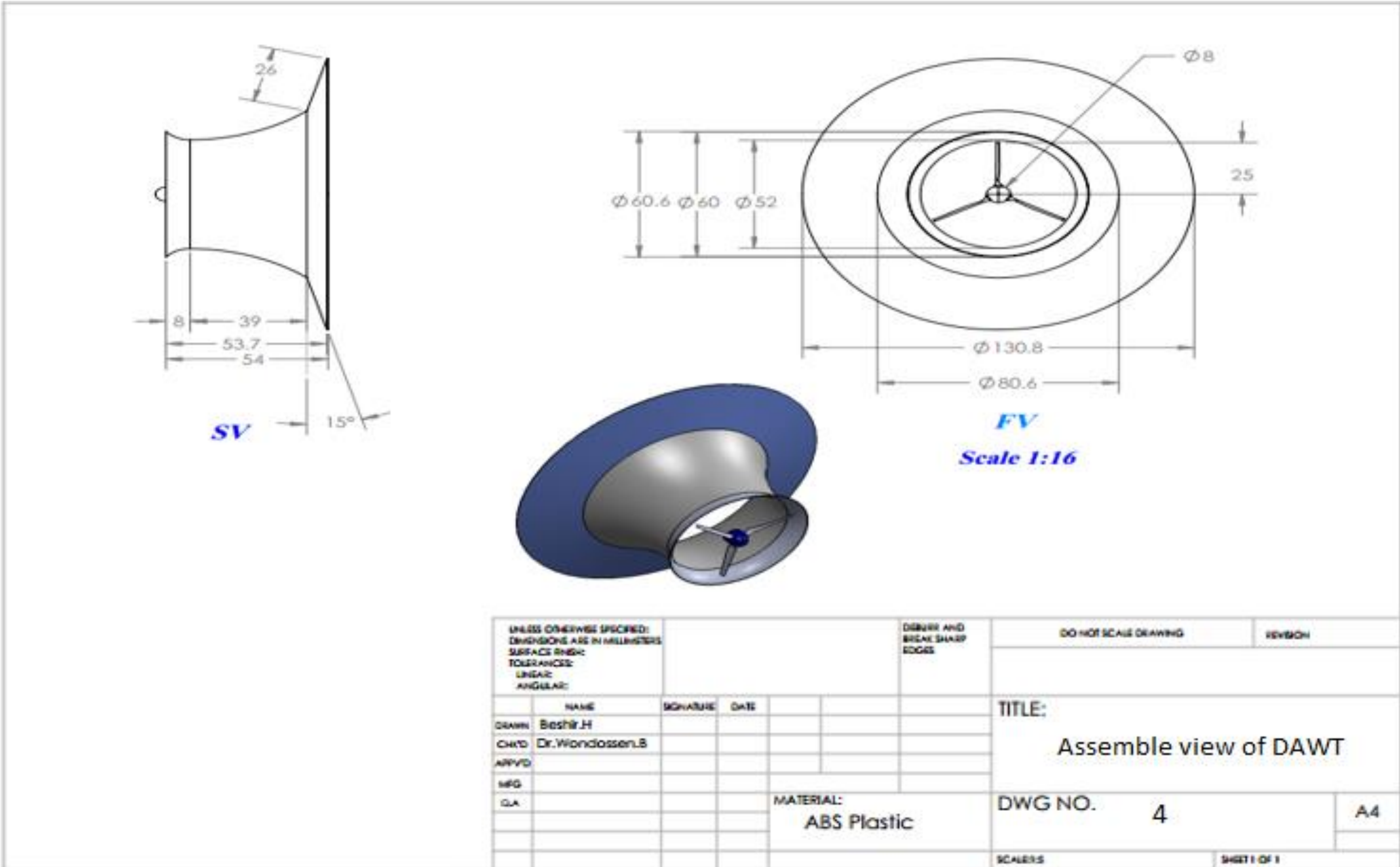
26
8
39
53.7
54
15°
SV
Ø8
25
Ø60.6 Ø60 Ø52
Ø130.8
Ø80.6
FV
Scale 1:16
UNLESS OTHERWISE SPECIFIED:
DIMENSIONS ARE IN MILLIMETERS
SURFACE FINISH:
TOLERANCES:
LINEAR:
ANGULAR:
DEBURR AND BREAK SHARP EDGES
DO NOT SCALE DRAWING
REVISION
NAME
SIGNATURE
DATE
DRAWN Beshir.H
CHK'D Dr.Wondossen.B
APPV'D
MFG
Q.A
MATERIAL:
ABS Plastic
TITLE:
Assemble view of DAWT
DWG NO.
4
A4
SCALE:1:5
SHEET 1 OF 1